Synthesis and Structural Characterization of Dinitrogen Chromium Complexes with Triamidoamine Ligands Possessing Bulky Substituents, and Nitrogen Fixation by These Complexes

Takeru Kuribayashi , Yoshiaki Kokubo , Haruki Nagai , Tomoya Furui , Tomohiro Ozawa , Hideki Masuda , Yuji Kajita *

Posted Date: 16 December 2025

doi: 10.20944/preprints202512.1439.v1

Keywords: nitrogen fixation; chromium; potassium; triamidoamine ligand; X-ray structure

Article

Synthesis and Structural Characterization of Dinitrogen Chromium Complexes with Triamidoamine Ligands Possessing Bulky Substituents, and Nitrogen Fixation by These Complexes

Takeru Kuribayashi [1], Yoshiaki Kokubo [1], Haruki Nagai [2], Tomoya Furui [2], Tomohiro Ozawa [2], Hideki Masuda [1,2,3] and Yuji Kajita [1,*]

[1] Graduate School of Engineering, Aichi Institute of Technology, Yakusa, Toyota 470-0392, Japan
[2] Graduate School of Engineering, Nagoya Institute of Technology, Gokiso-cho, Showa-ku, Nagoya 466-8555, Japan
[3] Department of Pharmaceutical Science, Suzuka University of Medical Science, Minami-tamagaki-cho, Suzuka 513-8670, Japan
* Correspondence: ykaji1974@aitech.ac.jp; Tel.: +81-565-48-8121

Abstract

Chromium complexes with triamidoamine derivatives bearing bulky substituents at the terminal positions of the ligands, tris(2-(3-pentylamino)ethyl)amine (**H$_3$L^{Pen}**) and tris(3-dicyclohexylmethylaminoethyl)amine (**H$_3$L^{Cy}**), have been prepared: [{Cr(**L^{Pen}**)}$_2$(μ-N$_2$)] (**1**), [{CrK(**L^{Pen}**)(μ-N$_2$)(Et$_2$O)}$_2$] (**2**), [CrCl(**L^{Pen}**)] (**3**), [Cr(**L^{Cy}**)] (**4**), [CrK(**L^{Cy}**)(μ-N$_2$)(18–crown–6)(THF)] (**5(THF)**), and [CrCl(**L^{Cy}**)] (**6**)). The preparation of these complexes has been confirmed by X-ray diffraction analysis. Complexes **1**, **2**, and **5(THF)** have coordinated dinitrogen molecules, with N–N bond lengths of 1.185(3), 1.174(9), and 1.162(3) Å, respectively. These lengths are significantly elongated compared to that of free dinitrogen molecule (1.10 Å), indicating that the N$_2$ ligands are activated. The ν(^{14}N–^{14}N) values of **1**, **2**, and **5(THF)** are 1715 cm^{-1} (ν(^{15}N–^{15}N): 1651 cm^{-1}) for **1** (Raman, in solution), 1787, 1743 cm^{-1} (ν(^{15}N–^{15}N) 1728, 1687 cm^{-1}) for **2** (IR, in solid), and 1824 cm^{-1} (ν(^{15}N–^{15}N) 1757 cm^{-1}) for **5(THF)** (IR, in solid), respectively. These values are markedly smaller than free nitrogen (2331 cm^{-1}), confirming that the dinitrogen is interacting with the metal ions and activated. The structures of **2** and **5(THF)** in solution have also been studied by ^{1}H NMR and solution IR spectroscopies. ^{1}H NMR spectra of these complexes have revealed that the peaks of **2** and **5(THF)** have been observed in the diamagnetic region, whereas those for the other complexes (**1**, **3**, **4**, and **6**) have exhibited paramagnetic shifts. The reactions of these complexes with K[C$_{10}$H$_8$] and HOTf under N$_2$ in THF have yielded hydrazine and a small amount of ammonia, however, they have not been catalytic. The ^{1}H NMR and IR spectra of the products obtained by reacting **1** or **3** with reductant K in THF under N$_2$ atmosphere have indicated that **2** has been formed based on spectral agreement. Similarly, upon examining for **4** or **6**, it has been confirmed that a species similar to **5(THF)** has been generated.

Keywords: nitrogen fixation; chromium; potassium; triamidoamine ligand; X-ray structure

1. Introduction

Nitrogen fixation occurs primarily in nature *via* nitrogenase enzymes and industrially through the Haber-Bosch process [1,2]. However, as the Haber-Bosch process requires high-temperature, high-pressure reaction conditions and hydrogen derived from fossil fuels, active research is

 doi:10.20944/preprints202512.1439.v1

underway into nitrogen fixation under milder conditions without hydrogen as the proton source [3]. Among various studies on nitrogen fixation, research on dinitrogen activation using transition metal complexes has been vigorously pursued since the Schrock's group first succeeded in catalytic nitrogen fixation using complexes centered on molybdenum, the metal present in nitrogenase enzymes [4–29].

Group VI metals such as molybdenum and tungsten are frequently employed as representative transition-metal complexes for dinitrogen activation, and highly interesting researches have been reported to date [12,13,16,18,20,29–41]. However, research utilizing chromium, which also belongs to Group VI, has been scarcely conducted; consequently, studies on the activation of dinitrogen molecules using chromium are highly significant [29,42–70]. Among these, although few in number, the dinitrogen activation reactions using chromium complexes have been reported, with some reporting the production of ammonia, hydrazine, hydrazine derivatives, or tris(trimethylsilyl)amine ($N(SiMe_3)_3$) [44,46–49,52,55,56,58–70]. The oxidation states of the chromium ions in these chromium-dinitrogen complexes are primarily I, II or III. However, recently, dinitrogen complexes in which the formal oxidation state of the chromium ion is –I have been reported [63]. We also synthesized several dinitrogen complexes containing Cr(IV) ions, which had not previously been used to activate dinitrogen, and reported that these complexes react with a proton source to produce ammonia and hydrazine [71]. However, as numerous unknowns remain in research concerning dinitrogen activation using chromium ions, further studies on dinitrogen activation employing diverse chromium ions are required.

Previously, we synthesized and structurally characterized dinitrogen chromium(IV) complexes bearing triamidoamine ligands and investigated their nitrogen fixation reactions yielding ammonia and hydrazine. However, the terminal substituent of the triamidoamine ligand was limited to a benzyl group. Therefore, in this study, the terminal substituents of the ligands were changed to the bulky tren derivatives, tris(2-(3-pentylamino)ethyl)amine ($\mathbf{H_3L^{Pen}}$) and tris(3-dicyclohexylmethylaminoethyl)amine ($\mathbf{H_3L^{Cy}}$), and the effect of substituents on chemical properties and reactivities with dinitrogen were investigated.

2. Results and Discussion

2.1. Preparation of Bulky Tren Ligands and Their Chromium Complexes, 1, 2, 3, 4, 5(THF), and 6

Two tren derivatives with bulky substituents, $\mathbf{H_3L^{Pen}}$ and $\mathbf{H_3L^{Cy}}$, were synthesized by the previously reported method, and several chromium complexes were prepared using these ligands [72]. These tren derivatives were lithiated with 3 equivalents of *n*-BuLi, yielding $Li_3[\mathbf{L^{Pen}}]$ and $Li_3[\mathbf{L^{Cy}}]$, respectively.

$Li_3[\mathbf{L^{Pen}}]$ reacted with $CrCl_3$ in Et_2O under N_2 to yield the dinitrogen dichromium complex, $[\{Cr(\mathbf{L^{Pen}})\}_2(\mu\text{-}N_2)]$ (**1**) (Scheme 1). Recrystallization of complex **1** from Et_2O solution gave dark red crystals. Reacting complex **1** with 10 equivalents of K metal in Et_2O under N_2 atmosphere yielded the dichromium complex containing two dinitrogen ligands and two K^+ ions, $[\{CrK(\mathbf{L^{Pen}})(\mu\text{-}N_2)(Et_2O)\}_2]$ (**2**) (Scheme 1). Recrystallization of complex **2** from Et_2O solution gave dark green crystals. The Cr(IV) complex bearing Cl^- ions, $[CrCl(\mathbf{L^{Pen}})]$ (**3**), was also synthesized as the Cr(IV) complex without dinitrogen ligands by the previously reported method [71].

On the other hand, reacting $Li_3[\mathbf{L^{Cy}}]$ with $CrCl_3$ in THF under N_2 afforded the mononuclear chromium complex $[Cr(\mathbf{L^{Cy}})]$ (**4**), which lacks a dinitrogen ligand. Recrystallizing complex **4** from *n*-hexane solution yielded dark red crystals. Reacting complex **4** with K metal and 18–crown–6 ether in THF under N_2 atmosphere gave the dinitrogen chromium complex containing a K^+ ion, $[CrK(\mathbf{L^{Cy}})(\mu\text{-}N_2)(18\text{–crown–}6)(THF)]$ (**5(THF)**) (Scheme 2). The Cr(IV) complex bearing Cl^- ion, $[CrCl(\mathbf{L^{Cy}})]$ (**6**), was also synthesized as the Cr(IV) complex without dinitrogen ligands by the same method as **3** (Scheme 3). Recrystallization of complex **6** from cyclopentylmethyl ether solution yielded dark violet crystals.

Preprints.org (www.preprints.org) | NOT PEER-REVIEWED | Posted: 16 December 2025 doi:10.20944/preprints202512.1439.v1

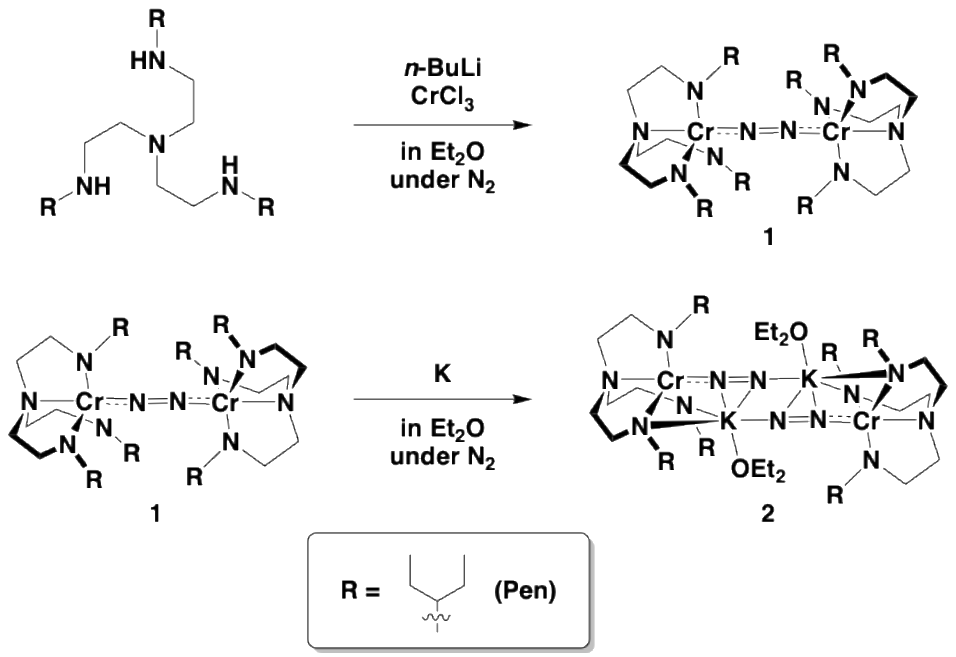

Scheme 1. Synthetic scheme of **1** and **2.**

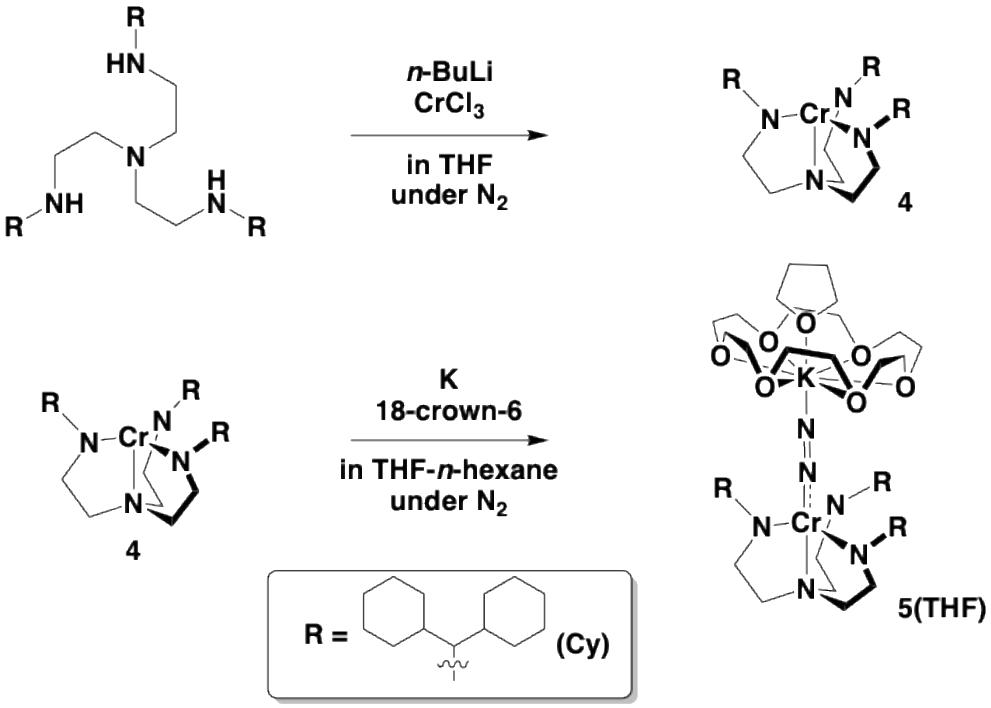

Scheme 2. Synthetic scheme of **4** and **5(THF)**.

 doi:10.20944/preprints202512.1439.v1

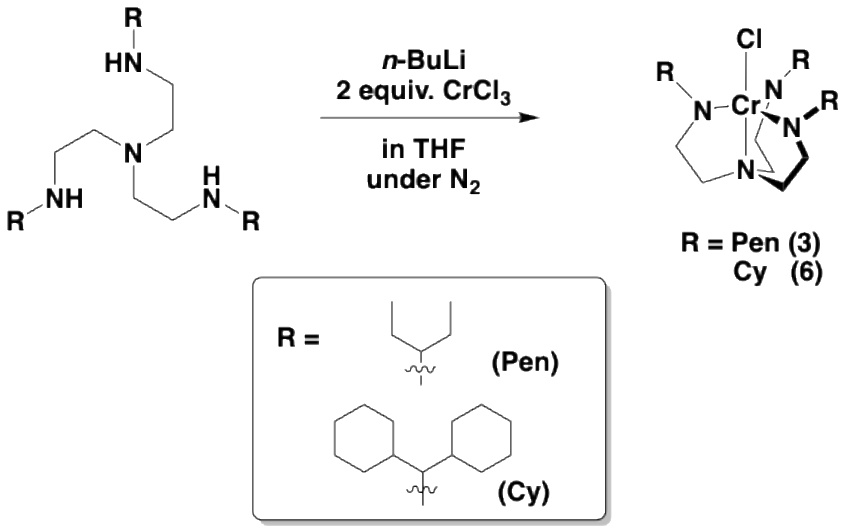

Scheme 3. Synthetic scheme of **3** and **6**.

2.2. Crystal Structures of Complexes 1, 2, 4, and 5(THF)

Crystal structures of **1** and **2** are shown in Figure 1 together. The crystal parameters and the selected bond lengths and angles of **1** and **2** are listed in Tables S1 and 1, respectively. Complex **1** is a dichromium complex possessing a dinitrogen ligand as the bridging ligand. Each Cr atom forms a trigonal bipyramidal geometry with three amido nitrogen atoms of $[\mathbf{L}^{\mathbf{Pen}}]^{3-}$ located on a trigonal plane and another amino nitrogen of $[\mathbf{L}^{\mathbf{Pen}}]^{3-}$ and dinitrogen molecule at the axial positions. The N–N bond length is 1.185(3) Å, which is significantly elongated compared to free nitrogen molecule (1.10 Å) [20], and is almost identical to those (1.188(4) and 1,185(7) Å) of the previously reported complex bearing a benzyl group as the substituent on the triamidoamine ligand ($[\mathbf{L}^{\mathbf{Bn}}]^{3-}$), $[\{Cr(\mathbf{L}^{\mathbf{Bn}})\}_2(\mu\text{-}N_2)]$ (Figure 2) [71]. The Cr–N_{N2} bond length of **1** is 1.8468(15) Å, which is longer than those (1.805(2) and 1.804(4) Å) of the previously reported dichromium complex with benzyl groups. This is thought to be due to the increased steric repulsion resulting from the pentyl group having greater spatial extension than the benzyl group. Therefore, the Cr–N_{N2} bond of **1** is considered to possess the properties of a weak multiple bond. Furthermore, the N–N distance is shorter than that (1.226(3) Å) of the dinitrogen-divanadium complex with the same triamidoamine ligand [72]. This is thought to be due to the difference in the back-donating ability of the metal ions to the dinitrogen ligand. That is: When the π-back donation is large, electrons enter the antibonding orbitals of dinitrogen from the metal, weakening the N–N bond and then reducing the ν(N–N) stretching vibration. Comparing dinitrogen-dichromium complex **1** and dinitrogen-divanadium complex [72], the ν(N–N) stretching vibration in the dichromium complex is 1715 cm^{-1}, while in the divanadium complex it is 1412 cm^{-1}, indicating the divanadium complex is more weakened. This indicates that the π-back-donation is larger in the dinitrogen-divanadium complex than in the dinitrogen-dichromium complex. Consequently, the M–N_{N_2} distance in the divanadium complex should be shorter than in the dichromium complex. Indeed, the V–N_{N_2} bond distance (1.7935(14)) Å is shorter than the Cr–N_{N_2} bond (1.8468(15) Å), clearly reflecting the difference in the π-back donating ability of the metal ions.

Complex **2** is a dinuclear Cr complex containing two potassium ions and two dinitrogen molecules. Each Cr atom forms a trigonal bipyramidal structure coordinated with the ligand $[\mathbf{L}^{\mathbf{Pen}}]^{3-}$ and dinitrogen molecule, similar to complex **1**. The dinitrogen ligand formed a bridge between the chromium and the two potassium ions, coordinating with one potassium ion in an end-on mode and with the other potassium ion in a side-on mode. The N–N bond length in **2** is 1.172(9) Å, showing a tendency to be shorter than that of **1**. This N–N bond length is longer than that (1.1624(19) Å) observed in the previously reported complex $[\{CrNa(\mathbf{L}^{\mathbf{Bn}})(\mu\text{-}N_2)(Et_2O)\}_2]$ (Figure 2) [71], which possesses a similar structure with terminal substituents of a benzyl group and a sodium ion, but with a potassium ion substituted instead. This is thought to be due to the large ionic radius of the potassium ion (1.37–1.64 Å) in comparison with sodium ion (0.99–1.39 Å) [73]. The potassium ion sandwiched between

 doi:10.20944/preprints202512.1439.v1

the two amido nitrogen atoms of the ligand migrated towards the dinitrogen ligand, resulting in one dinitrogen ligand forming coordination bonds with two potassium ions. The Cr–N_{N2} bond length is 1.762(8) Å, indicating that **2** has stronger multiple bond character than **1**.

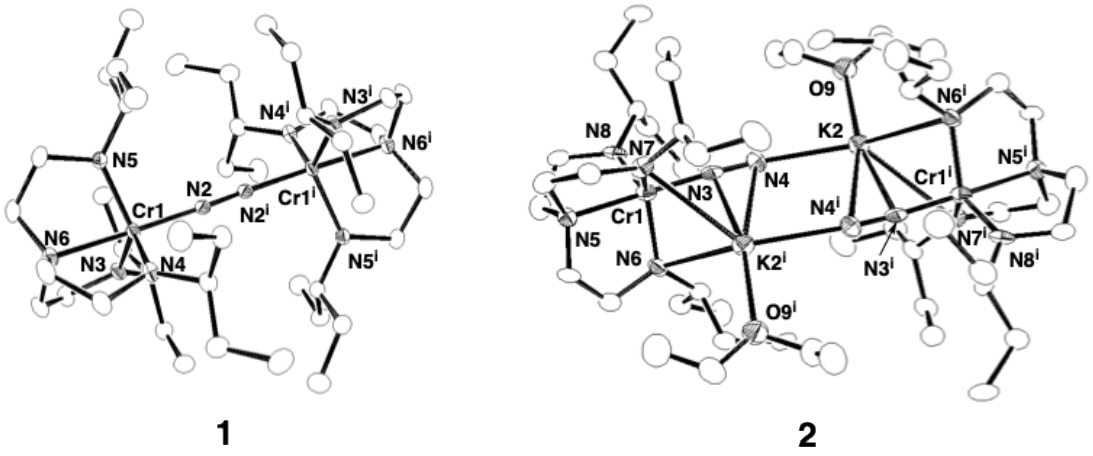

Figure 1. ORTEP views of **1** and **2** with atomic numbering scheme (50 % probability thermal ellipsoids). Hydrogen atoms are omitted for clarity. For complex **1**, the atoms with and without superscript i are related by a center of symmetry each other (1/2 – *x*, 3/2 – *y*, 1 – *z*). For complex **2**, the atoms with and without superscript i are related by a center of symmetry each other (1 – *x*, 1 – *y*, 1 – *z*).

Table 1. Selected Bond Lengths (Å) and Angles (deg) for **1** and **2.**

			1		
Cr1–N2	1.8468(15)	Cr1–N3	1.8965(16)	Cr1–N4	1.8906(18)
Cr1–N5	1.8876(17)	Cr1–N6	2.1110(17)	N2–N2^{i}	1.185(3)
Cr•••Cr^{i}	4.8774(7)				
N2–Cr1–N3	98.11(7)	N2–Cr1–N4	99.76(7)	N2–Cr1–N5	97.25(7)
N2–Cr1–N6	177.95(7)	N3–Cr1–N4	117.87(7)	N3–Cr1–N5	118.37(7)
N3–Cr1–N6	80.89(7)	N4–Cr1–N5	117.51(7)	N4–Cr1–N6	82.29(7)
N5–Cr1–N6	81.71(7)	N2^{i}–N2–Cr1	177.1(2)		
			2		
Cr1–N3	1.762(8)	Cr1–N5	2.096(7)	Cr1–N6	1.931(7)
Cr1–N7	1.901(8)	Cr1–N8	1.857(8)	N3–N4	1.174(9)
N3–K2^{i}	2.870(8)	N4–K2^{i}	3.101(8)	N6–K2^{i}	2.983(8)
N7–K2^{i}	3.108(7)	N4–K2	2.658(8)	K2–O9	2.722(7)
Cr1•••K2^{i}	3.252(3)	Cr•••K2	5.551(3)		
N3–Cr1–N5	179.0(3)	N3–Cr1–N6	96.7(3)	N3–Cr1–N7	96.9(3)
N3–Cr1–N8	97.2(3)	N5–Cr1–N6	82.5(3)	N5–Cr1–N7	83.0(3)
N5–Cr1–N8	83.8(3)	N6–Cr1–N7	115.9(3)	N6–Cr1–N8	121.4(3)
N7–Cr1–N8	118.4(3)	N3–K2^{i}–N4	22.25(18)	N3–K2^{i}–N4^{i}	100.7(2)
N3–K2^{i}–N6	56.3(2)	N3–K2^{i}–N7	54.4(2)	N3–K2^{i}–O9^{i}	167.0(2)
N4–K2^{i}–N4^{i}	78.5(2)	N4–K2^{i}–N6	74.1(2)	N4–K2^{i}–N7	132.5(2)
N4–K2^{i}–O9^{i}	166.4(2)	N4^{i}–K2^{i}–N6	139.9(2)	N4^{i}–K2^{i}–N7	132.5(2)
N4^{i}–K2^{i}–O9^{i}	90.7(2)	N6–K2^{i}–N7	64.4(2)	N6–K2^{i}–O9^{i}	110.7(2)
N7–K2^{i}–O9^{i}	121.2(2)	N4–N3–Cr1	175.6(7)	N3–N4–K2	168.5(7)

 doi:10.20944/preprints202512.1439.v1

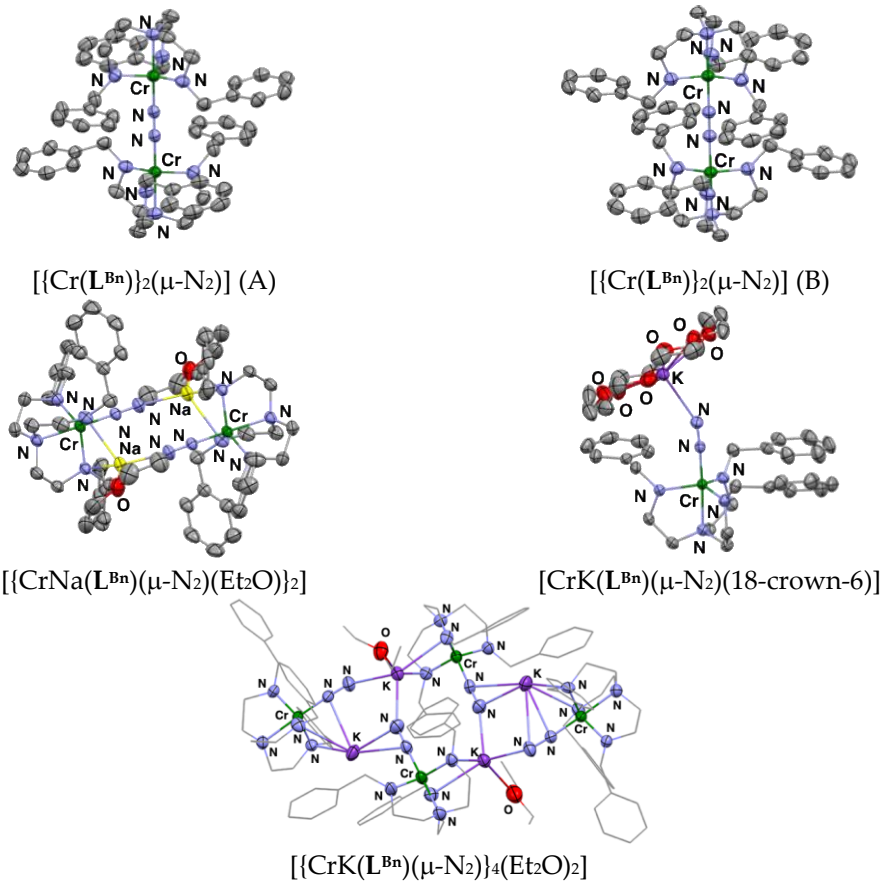

Figure 2. Molecular structures of the previously reported chromium-dinitrogen complexes with $[\mathbf{L}^{Bn}]^{3-}$ ligand (50 % thermal ellipsoids) for comparison. For $[\{Cr(\mathbf{L}^{Bn})\}_2(\mu\text{-}N_2)]$, two independent complexes, $[\{Cr(\mathbf{L}^{Bn})\}_2(\mu\text{-}N_2)]$ (A) and $[\{Cr(\mathbf{L}^{Bn})\}_2(\mu\text{-}N_2)]$ (B), are contained in the unit cell. Hydrogen atoms in all structures are omitted and carbon atoms in $[\{CrK(\mathbf{L}^{Bn})(\mu\text{-}N_2)\}_4(Et_2O)_2]$ are drawn as wireframe for clarity. These structural data are given in reference 71.

For complex **4** synthesized using $Li_3[\mathbf{L}^{Cy}]$, accurate results could not be obtained from X-ray crystal structure analysis. However, because the approximate structure was already known, 25% probability ellipsoids are displayed for the carbon, nitrogen, and chromium atoms in the ORTEP display of **4** (Figure 3). The crystal parameters and the selected bond lengths and angles of **4** are listed in Tables S1 and S2, respectively. Complex **4** revealed a trigonal monopyramidal coordination geometry, with the axial position being vacant. The chromium complex with a similar structure has previously been reported by Filippou's group [74]. Also, the previously reported vanadium complex with the same ligand, $[V(\mathbf{L}^{Cy})]$ [72], also possessed an axial vacancy, but one cyclohexane ring was positioned axially, thereby preventing the coordination of other molecules. In contrast, the cyclohexane ring in complex **4** is not located axially, resulting in a structure with many gaps, as shown in Figure 4. Consequently, complex **4** is very air sensitive.

 doi:10.20944/preprints202512.1439.v1

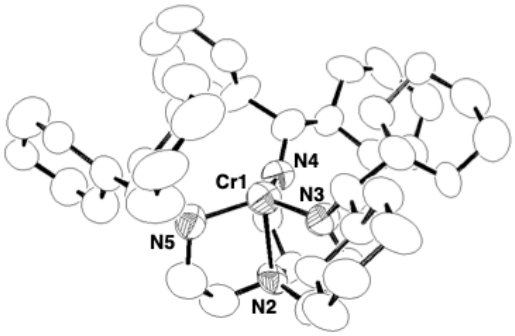

4

Figure 3. ORTEP view of **4** with atom numbering scheme (25 % probability thermal ellipsoids). Hydrogen atoms are omitted for clarity.

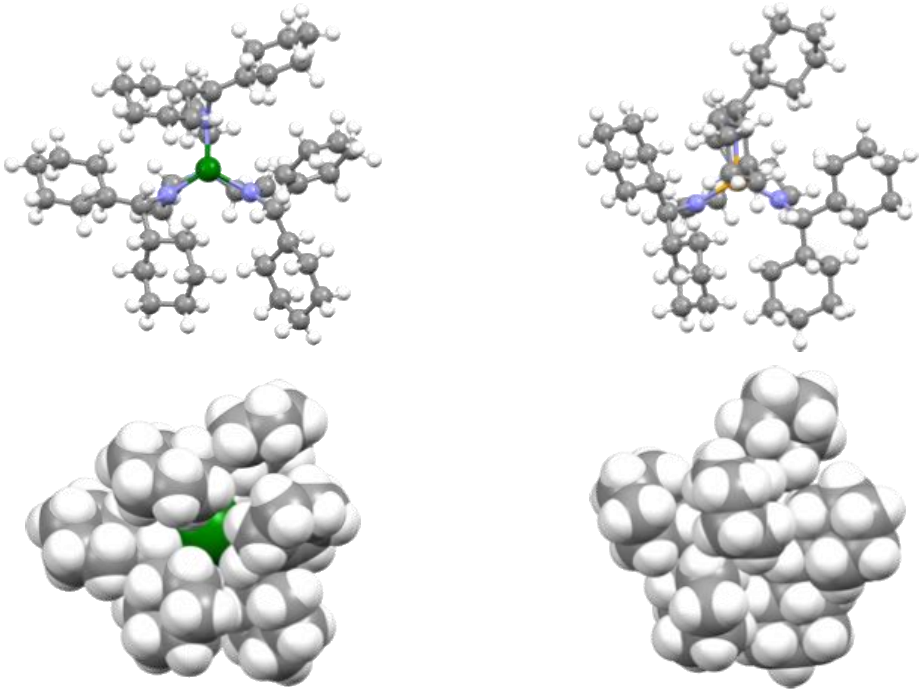

[Cr(**L**^{Cy})] (**4**) [V(**L**^{Cy})]

Figure 4. Ball and stick (top) and space-filling models (bottom) of [Cr(**L**^{Cy})] (**4**) (left side) and the previously reported [V(**L**^{Cy})] (right side) (C, H, N, Cr, and V are shown in gray, white, blue, green, and orange colors, respectively). The structural data of [V(**L**^{Cy})] is given in reference number 72.

Next, reacting complex **4** with metallic potassium and 18-crown-6 ether under N_2 yielded the dinitrogen chromium complex **5(THF)**. Fortunately, a single crystal of **5(THF)** was obtained from THF-*n*-hexane solution and analyzed by X-ray diffraction. The crystal structure is shown in Figure 5, and the crystal parameters and the selected bond lengths and angles are listed in Tables S1 and 2, respectively. The Cr complex adopts a trigonal bipyramidal structure, forming a trigonal plane with three amido nitrogen atoms of [**L**^{Cy}]$^{3-}$ ligand, with the axial positions occupied by another amine nitrogen of [**L**^{Cy}]$^{3-}$ ligand and a dinitrogen ligand. The opposite side of the dinitrogen ligand is bonded to a potassium ion coordinated by an 18-crown-6 ether ligand from the planar side and a THF molecule from the apical position, resulting in the N_2 ligand forming a bridge between the chromium and potassium atoms, with an N–N bond length of 1.162(3) Å. The N–N bond length is slightly shorter than that (1.167(2) Å) of the previously reported chromium–dinitrogen complex containing a benzyl group, [CrK(**L**^{Bn})(μ-N_2)(18-crown-6)] (Figure 2) [71]. The Cr–N_{N2} and K–N_{N2} bond lengths of **5(THF)** were 1.761(2) and 2.647(2) Å, respectively. These bond lengths were also shorter compared

 doi:10.20944/preprints202512.1439.v1

with the Cr–N_{N2} (1.7678(15) Å) and K–N_{N2} bond lengths (2.7822(16) Å) of the previously reported chromium complex [CrK($\mathbf{L}^{Bn}$)(μ-N_2)(18-crown-6)] [71].

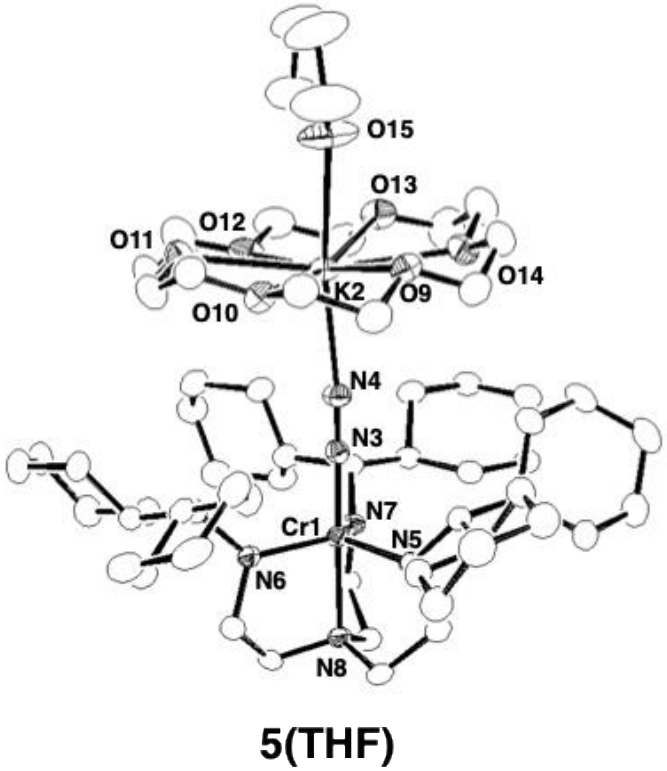

Figure 5. ORTEP view of **5(THF)** with atom numbering scheme (50 % probability thermal ellipsoids). Hydrogen atoms are omitted for clarity.

Table 2. Selected Bond Lengths (Å) and Angles (deg) for **5(THF).**

5(THF)					
Cr1–N3	1.761(2)	Cr1–N5	1.912(2)	Cr1–N6	1.911(2)
Cr1–N7	1.907(2)	Cr1–N8	2.125(2)	K2–N4	2.647(2)
K2–O9	2.867(2)	K2–O10	2.775(2)	K2–O11	2.866(2)
K2–O12	2.767(2)	K2–O13	2.852(2)	K2–O14	2.774(2)
K2–O15	2.707(2)	N3–N4	1.162(3)	Cr1•••K2	5.5547(8)
N3–Cr1–N5	97.44(10)	N3–Cr1–N6	97.40(9)	N3–Cr1–N7	96.46(10)
N3–Cr1–N8	179.24(9)	N5–Cr1–N6	118.77(9)	N5–Cr1–N7	119.16(9)
N5–Cr1–N8	82.52(9)	N6–Cr1–N7	117.56(10)	N6–Cr1–N8	83.27(9)
N7–Cr1–N8	82.91(9)	N4–N3–Cr1	179.6(3)	N4–K2–O9	100.44(7)
N4–K2–O10	95.50(7)	N4–K2–O11	101.65(7)	N4–K2–O12	87.16(7)
N4–K2–O13	96.66(7)	N4–K2–O14	91.30(7)	N4–K2–O15	172.33(9)
N3–N4–K2	171.8(2)				

2.3. Crystal Structures of Complexes 3 and 6

The crystal structure of $Cr^{IV}Cl$ complex with $[\mathbf{L}^{Pen}]^{3-}$ or $[\mathbf{L}^{Cy}]^{3-}$, **3** or **6**, is shown in Figure 6 together, and the crystal parameters and the selected bond lengths and angles are listed in Tables S1 and 3, respectively. Crystal structural data for **3** has been reported previously [71] and the ORTEP views are also shown in Figure 6 of this paper. The coordination structures around the Cr ion in **3**

 doi:10.20944/preprints202512.1439.v1

and **6** have both trigonal bipyramidal geometry. The three amine nitrogen atoms of the bulky ligand are arranged in a triangular plane around Cr atom, while another amido nitrogen atom of the ligand and the chlorine atom are positioned axially. The Cr–Cl bond lengths in **3** and **6** are almost the same (2.3145(6) Å for **3**, 2.3147(7) Å for **6**). However, comparing the Cr–N_{amine} and Cr–N_{amido} bond lengths in these complexes, the Cr–N_{amine} (2.0446(16) Å) and Cr–N_{amido} (av) (1.866 Å) of **3** are shorter than those (Cr–N_{amine} 2.088(2) Å, Cr–N_{amido} (av) 1.8828 Å) in **6**. This is thought to be due to the steric repulsion between the terminal substituents of the ligand in **6** being greater than that in **3**. Previously, Filippou's group has reported a similar chromium complex with terminal trimethylsilyl groups on the triamidoamine ligand, however, no structural trend could be found among these three Cr(IV)–Cl complexes [74].

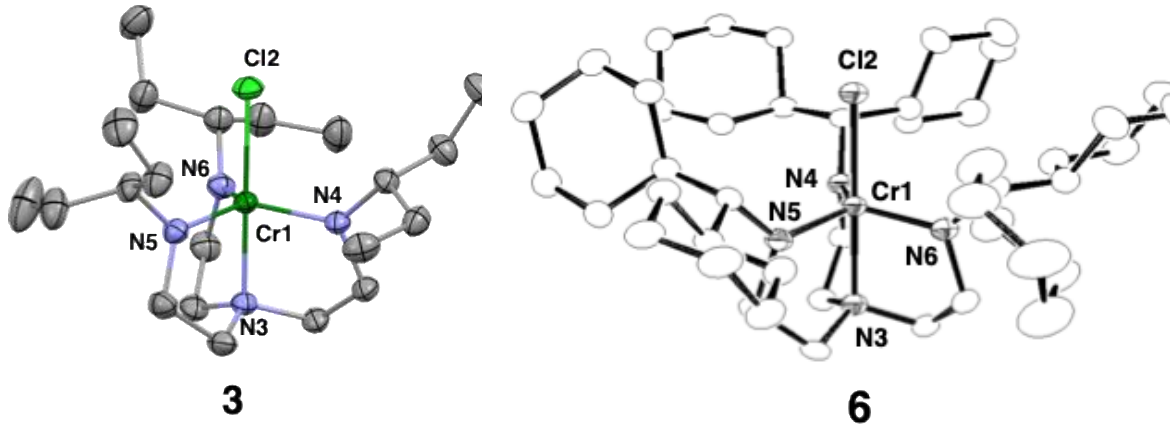

Figure 6. Molecular structure of **3** and ORTEP view of **6** with the atom numbering scheme (50 % probability thermal ellipsoids). Hydrogen atoms are omitted for clarity. The molecular structure for **3** shows modified atomic numbering from the original in the previously reported paper [71].

Table 3. Selected Bond Lengths (Å) and Angles (deg) for **3** and **6.**

		3 [a]			
Cr1–Cl2	2.3145(6)	Cr1–N3	2.0446(16)	Cr1–N4	1.8661(16)
Cr1–N5	1.8680(17)	Cr1–N6	1.8650(17)		
Cl2–Cr1–N3	179.51(5)	Cl2–Cr1–N4	96.55(5)	Cl2–Cr1–N5	97.03(5)
Cl2–Cr1–N6	97.09(6)	N3–Cr1–N4	82.98(7)	N3–Cr1–N5	83.08(7)
N3–Cr1–N6	83.28(7)	N4–Cr1–N5	119.03(8)	N4–Cr1–N6	119.39(7)
N5–Cr1–N6	117.32(8)				
		6			
Cr1–Cl2	2.3147(7)	Cr1–N3	2.088(2)	Cr1–N4	1.883(2)
Cr1–N5	1.8874(19)	Cr1–N6	1.878(2)		
Cl2–Cr1–N3	179.50(6)	Cl2–Cr1–N4	96.80(6)	Cl2–Cr1–N5	96.44(6)
Cl2–Cr1–N6	97.20(7)	N3–Cr1–N4	83.05(8)	N3–Cr1–N5	83.23(8)
N3–Cr1–N6	83.29(9)	N4–Cr1–N5	119.49(9)	N4–Cr1–N6	117.96(9)
N5–Cr1–N6	118.39(9)				

[a] The bond lengths and angles of **3** are described with modifications to the original atom numbering scheme reported in the previously paper [71].

2.4. Raman and IR Spectra of 1, 2, and 5(THF)

 doi:10.20944/preprints202512.1439.v1

To investigate the reactivity of the dinitrogen molecule bound to Cr atom in complexes **1**, **2**, and **5(THF)**, vibrational spectroscopic measurements were carried out on them. Complex **1** was studied by Raman spectroscopy in cyclohexane solution using laser light excited at 532 nm. The $\nu(^{14}N–^{14}N)$ stretching vibration of complex **1** was detected at 1715 cm^{-1}. When $^{15}N_2$ was used in the reaction instead of $^{14}N_2$, the $\nu(^{15}N–^{15}N)$ stretching vibration was obtained at 1651 cm^{-1}, exhibiting an ideal isotope shift (Figure S1). This value is significantly smaller than free dinitrogen (2331 cm^{-1}) [20], clearly indicating that the dinitrogen ligand has been activated, but it is larger than the $\nu(^{14}N–^{14}N)$ stretching vibration (1412 cm^{-1}) of the dinitrogen divanadium complex possessing the same triamidoamine ligand [72]. As mentioned in Section 2.1, this is also refelected in the N–N bond length and is thought to be due to the fact that the back-donation from the metal to the dinitrogen ligand is smaller for Cr than V.

Complexes **2** and **5(THF)**, which possess the dinitrogen ligands bridging between the chromium ion and potassium ion, were investigated by IR spectroscopy (ATR method). The peaks assignable to $\nu(^{14}N–^{14}N)$ stretching vibration were observed as two bands at 1787 and 1743 cm^{-1} for **2** (Figure S2), and as one band at 1824 cm^{-1} for **5(THF)** (Figure S3). When ^{15}N-labeled dinitrogen chromium complexes of **2** and **5**, $[\{CrK(\mathbf{L}^{Pen})(\mu\text{-}^{15}N_2)(Et_2O)\}_2]$ (**2′**) and $[CrK(\mathbf{L}^{Cy})(\mu\text{-}^{15}N_2)(18\text{-crown-6})(THF)]$ (**5′(THF)**), were employed, these peaks shifted to 1728 and 1687 cm^{-1} for **2′** and to 1757 cm^{-1} for **5′(THF)**, respectively. These findings indicate that the stretching vibration frequencies of dinitrogen molecules have shifted to the lower energy side due to the isotope effect, and the presence of two peaks in **2** suggests that dinitrogen exists in two different bridging modes between Cr and K. In the previously reported complex $[\{CrNa(\mathbf{L}^{Bn})(\mu\text{-}N_2)(Et_2O)\}_2]$, which possesses a sodium ion instead of a potassium ion and features benzyl groups at the terminals of the triamidoamine ligand, the $\nu(^{14}N–^{14}N)$ stretching vibration was observed at 1813 cm^{-1} [71]. Therefore, based on the crystal structure of **2** described in Section 2.2 (Figure 1), the two peaks detected at 1787 and 1743 cm^{-1} for **2** are considered to correspond to the dinitrogen ligand bridged by a chromium ion and one potassium ion in an end-on mode, and the dinitrogen ligand bridged by a chromium ion and two potassium ions in an end-on and a side-on modes, respectively.

The ν(N–N) stretching vibration (1824 cm^{-1}) of **5(THF)** was observed in a higher energy region than that (1807 cm^{-1}) of the previously reported complex $[CrK(\mathbf{L}^{Bn})(\mu\text{-}N_2)(18\text{-crown-6})]$ [71]. This is consistent with the elongated N–N bond lengths of the respective complexes being 1.162(3) Å for **5(THF)** and 1.167(2) Å for $[CrK(\mathbf{L}^{Bn})(\mu\text{-}N_2)(18\text{-crown-6})]$, respectively, with complex **5(THF)** exhibiting a slightly shorter bond length [71].

2.5. IR Spectra of 2 and 5(THF) in Solution

To further elucidate the structures of **2** and **5(THF)** in solution, the IR spectra were measured in toluene and THF. Those of **2** are shown in Figures S4 and S5, respectively, and those of **5(THF)** are shown in Figures S6 and S7, respectively. The ν(N–N) stretching vibration peaks of **2** appeared as a single peak at 1790 in toluene and at 1805 cm^{-1} in THF, respectively. However, in the solid state, as mentioned above, two peaks (1787 and 1743 cm^{-1}) were observed in the lower energy region compared to the solution state. This finding suggests that the dinitrogen ligand in solution is bridging between the K^+ ion and the Cr(IV) ion in end-on fashion, although the dinitrogen ligands in the crystal structure of **2** involved in both end-on and side-on fashions.

On the other hand, for complex **5(THF)**, the ν(N-N) stretching vibration peak was observed as a single peak at 1805 cm^{-1} in toluene (Figure S6) and at 1809 cm^{-1} in THF (Figure S7), respectively, both of which were observed in lower energy side compared to that (1824 cm^{-1}) in the solid state. As explained in Section 2.6 below, in toluene or THF solution, the THF ligand is thought to be removed from complex **5(THF)**, forming a THF-free complex **5**.

2.6.15. N NMR Spectra of 2 and 5(THF)

To further examine the coordination mode of dinitrogen molecules with Cr atom in complexes **2** and **5(THF)** in solution, ^{15}N NMR spectra were measured in C_6D_6 solution using complexes **2′** and

 doi:10.20944/preprints202512.1439.v1

5′(THF) with ^{15}N-labeled N_2. The peaks of ^{15}N-labeled dinitrogen ligands in both complexes were observed at –1.9 and –32 ppm for **2′** (Figure S8), and at 8.8 and –27.5 ppm for **5′(THF)** (Figure S9). The peaks in low and high magnetic field regions for **2'** and **5' (THF)** are well consistent with those of the previously reported chromium complexes [{CrK($\mathbf{L}^{Bn}$)(μ-N_2)}$_4$(Et_2O)$_2$] (1.79 and –71.26 ppm) [71] and [CrK($\mathbf{L}^{Bn}$)(μ-N_2)(18-crown-6)] (4.79 and –25.22 ppm) [71], so they were assigned to the N_α atom bonded to Cr on the low magnetic field side of the coordinated N_2, and to the N_β atom on the opposite side on the high magnetic field side, respectively. The two peaks in complex **2′** exhibited both small shoulder peaks on the lower magnetic field side. To investigate the reason, spectra were aquired by varying the number of scans (10,000, 20,000, 30,000, 40,000, and 50,000 scans). It was confirmed that the shoulder peaks gradually changed from a small double peak to a shoulder peak (Figure S10). Considering the IR spectral behavior of **2** described above, these peaks are likely to originate from species in which the dinitrogen ligand coordinates to the potassium ion in a side-on mode. Therefore, these spectra suggest that species in which the dinitrogen ligand coordinates to the potassium ion in the side-on mode are thermally unstable in solution and gradually transform into the end-on mode species.

By the way, in the spectrum of **5′(THF)** [CrK($\mathbf{L}^{Cy}$)(μ-$^{15}N_2$)(18–crown–6)(THF)], small peaks were observed at 5, –24, and –72 ppm. The peak at –72 ppm is thought to be due to the amine N atoms of the ligand [$\mathbf{L}^{Cy}$]$^{3-}$, because it exhibits the largest peak area among the three peaks. A single crystal was accidentally precipitated from the NMR sample tube used for the ^{15}N NMR spectral measurement of **5′(THF)**, so its crystal structure analysis was carried out. As a result, the THF ligand coordinated to the potassium ion in **5′(THF)** was removed, forming the complex [CrK($\mathbf{L}^{Cy}$)(μ-$^{15}N_2$)(18–crown–6)] (**5′**). The N–N bond length of the dinitrogen ligand in **5′** was slightly elongated from 1.162 (3) Å to 1.170 (4) Å as compared with that in **5′(THF)** (Figure S11, Table 2, and Table S3). Considering that most of THF ligands in **5(THF)** are removed even in THF solution, the fact that stretching vibrations in the low-energy region were observed in solution, as mentioned in Section 2.5 above, is consistent with the elongation of the N–N bond distance in the crystal structure. Therefore, the strong peaks at 8.8 and –27.5 ppm in ^{15}N NMR spectrum (Figure S9) of **5′(THF)** are thought to originate from the N_2 ligand of complex **5′** without bound THF. Furthermore, the minor peaks at 5 ppm and –24 ppm in Figure S9 are considered to originate from the N_2 ligand of a small amount of **5′(THF)** in which THF is coordinated to the potassium ion.

2.6.1. H NMR Spectra of 1 – 6

The ^1H NMR spectrum of **1** in C_6D_6 exhibited paramagnetic shifts with broadened peaks at 12, 5, 0.8, and –38 ppm (Figure S14). The magnetic moment (μ_{eff}) of **1** in solution was measured by the Evans method and estimated to be μ_{eff} = 2.87 μ_B at room temperature. This result suggests that the spin state of **1** is S = 1, similar to that of [{Cr($\mathbf{L}^{Bn}$)}$_2$(μ-N_2)] reported previously [71]. On the other hand, the peaks in ^1H NMR spectra of **2** (Figure S15) and **5(THF)** (Figure S18) in C_6D_6 were observed as simple spectra in the diamagnetic region, despite the complexity of their crystal structures. These findings clearly indicate that complexes **2** and **5(THF)** exhibit high symmetry, specifically C_3 symmetry, in solution. As mentioned above, in C_6D_6, most of the THF ligands in **5(THF)** were released, likely forming [CrK($\mathbf{L}^{Cy}$)(μ-$^{14}N_2$)(18-crown-6)] (**5**). And these are also consistent with those for the previously reported complexes, [{CrNa($\mathbf{L}^{Bn}$)(μ-N_2)}$_2$] and [CrK($\mathbf{L}^{Bn}$)(μ-N_2)(18-crown-6)], suggesting a very strong antiferromagnetic interaction between the Cr ion and the N_2 ligand with S = 0 spin state [71]. Furthermore, the ^1H peaks of ligands $\mathbf{H_3L}^{Pen}$ and $\mathbf{H_3L}^{Cy}$ were also observed in the ^1H NMR spectra of **2** and **5(THF)** (Figures S15 and S18). This indicates that these complexes are decomposed in solution at room temperature, even under anaerobic conditions.

The ^1H NMR spectra of **3** and **6** in C_6D_6 showed paramagnetic shifts with broadened peaks at 20, 12, 0.4, –36, and –69 ppm for **3** (Figure S16), and at 13, 3.6, 3.1, 1.7, 1.5, 1.4, 1.1 and –41 ppm for **6** (Figure S19). The magnetic moments (μ_{eff}) of these complexes in solution were estimated to be 2.84 and 2.96, respectively. Therefore, these complexes were shown to be high-spin d^2 metal complexes [71]. The ^1H NMR spectrum of Cr(III) complex **4** exhibited paramagnetism, with broadened peaks at

 doi:10.20944/preprints202512.1439.v1

3 – 0, –18, –35, and –66 ppm (Figure S17). The magnetic moment of **4** calculated by the Evans method was μ_{eff} = 3.82 μ_B at room temperature, corresponding to a spin state of S = 3/2. This value is very close to that reported previously by Filippou's group for a Cr(III) complex bearing a trimethylsilyl group as the terminal substituent of a triamidoamine ligand which has a structure similar to **4** (μ_{eff} = 3.8 μ_B) [74].

2.7. Comparison of Physico-chemical Properties (X-ray, Raman, IR, NMR) of 1, 2 and 5(THF) with Previously Reported Chromium Dinitrogen Complexes

The physicochemical properties (Cr–N_{N2}/Å, N–N/Å, ν(N–N)/cm^{-1}, ^{15}N NMR/ppm) of dinitrogen ligands coordinated to Cr complexes obtained in this study were compared with those of previously reported Cr complexes [71] to examine the relationships among them. The results are summarized in Table 3. We expected to observe the trans influence between the Cr–N_{N2} bond length and the N–N bond length, but no such an influence was observed. Rather, the longer the Cr–N_{N2} bond length between two Cr atoms, the longer the N–N bond length tended to be as well. Conversely, in Cr complexes with nitrogen ligands sandwiched between Cr and K, the Cr–N_{N2} bond length tended to be shorter, and the N–N bond length also tended to be shorter. In contrast, a reasonably consistent trend was observed between the N–N bond lengths and the ν(N–N) stretching vibrations. Especially, as the N–N bond length increased, the ν(N–N) stretching vibration decreased, and as the N–N bond length decreased, the ν(N–N) stretching vibration increased. This relationship has been reported previously [18] and is natural when considering the relationship between force and spring in vibrational phenomena.

Next, we considered that observing the NMR spectra of dinitrogen ligands bound to Cr would allow us to infer the electronic state of the bound N atom *of N_2 ligands*, and thus compared the ^{15}N peaks of the dinitrogen ligands in the chromium dinitrogen complexes. While the ^{15}N NMR spectrum of the N_2 molecule sandwiched between two Cr atoms was not measured, in the dinitrogen ligands sandwiched between Cr and K, a clear difference in chemical shifts was observed between N_α and N_β. This is because electrons flow from Cr to the N_2 molecule *via* a π-back bonding and the N_β atom, reduced by K, carries a negative charge. The nitrogen ligand forms an ionic bond with K^+, attracting electrons to N_β and increasing its negative charge, leading to the detection of N_b in high magnetic fields. The N_α signal observed on the low magnetic field side generally appears between approximately 9 ~ −2 ppm, though with some variation. In contrast, the N_β signal is observed on the high magnetic field side around –30 ppm. However, in the previously reported complex [{CrK(**L**^{Bn})(μ-N_2)}$_4$(Et_2O)$_2$], it was observed at −71 ppm, a significantly higher magnetic field side. This is likely due to a substantial accumulation of electron density on the N_β in this complex.

Table 3. Comparison of physicochemical properties (X-ray, Raman, IR, ^{15}N NMR) of dinitrogen-chromium complexes.

complex	Cr–N_{N2}/Å	N–N/Å	n(N–N)/cm^{-1}	^{15}N NMR/ppm	ref.
1 {Cr(**L**^{Pen})}$_2$(m–N_2)]	1.8468(15)	1.185(3)	1715	– [a]	this work
2 [{CrK(**L**^{Pen})(m–N_2)(Et_2O)}$_2$]	1.762(8)	1.174(9)	1787 1743	–1.9 –32	this work
5(THF) [CrK(**L**^{Cy})(m–N_2)(18-crown-6)(THF)]	1.762(3)	1.162(3)	1824 1757	8.8 –27.5	this work
[{Cr(**L**^{Bn})}$_2$(m–N_2)]	1.804(4) 1.805(2)	1.188(4) 1.185(7)	1772	– [a]	71
[{CrNa(**L**^{Bn})(m–N_2)(Et_2O)}$_2$]	1.755(3)	1.1624(19)	1813	– [a]	71
[{CrK(**L**^{Bn})(m–N_2)}$_4$(Et_2O)$_2$]	1.757(4) 1.751(4) 1.752(4) 1.758(4)	1.169(4) 1.182(4) 1.177(5) 1.166(4)	1804 1774	1.79 –71.26	71

 doi:10.20944/preprints202512.1439.v1

[CrK($\mathbf{L^{Bn}}$)(m–N_2)(18-crown-6)]	1.7678(15)	1.167(2)	1807	4.79 –25.22	71

[a] Not measured.

2.8. Reactions of Chromium Complexes with K[$C_{10}H_8$] and HOTf Under N_2

The reactions of complexes **1** – **6** with K[$C_{10}H_8$] and HOTf in THF were carried out under N_2 atmosphere, yielding hydrazine and a small amount of ammonia in all cases. The quantifications of hydrazine and ammonia were carried out using the ^{1}H NMR and *p*-dimethylaminobenzaldehyde methods, respectively. The quantification results and the details are shown in Tables 4 and S4, respectively. Table 4 presents also the results from the previously reported nitrogen fixation experiments using Cr(IV) complexes with [$\mathbf{L^{Bn}}$]$^{3-}$ ligand for comparison. Although the yields of ammonia and hydrazine produced in this study were both low in all complexes, hydrazine was formed in greater quantities than ammonia. Here, two interesting findings can be noticed from Table 4. They are described below.

Table 4. Quantification of ammonia and hydrazine produced from the reactions of **1** – **6** with K[$C_{10}H_8$] and HOTf under N_2[a].

complex	Yield (%) [b, c]		ref.
	NH_3	N_2H_4	
1	1.1	12.1	this work
2	1.5	11.1	this work
3	0.4	8.8	this work
4	0.3	22.8	this work
5(THF)	0.7	44.8	this work
6	1.3	6.4	this work
[Cr_2($\mathbf{L^{Bn}}$)$_2$(N_2)]	19.3	15.4	71
[{CrK($\mathbf{L^{Bn}}$)(N_2)}$_4$(Et_2O)$_2$]	26.7	15.2	71
[CrK($\mathbf{L^{Bn}}$)(N_2)(18-crown-6)]	29.0	12.8	71

[a] All reactions were carried out in THF at -78 °C under N_2. [b] Yields are given for a chromium ion, and these values are an average of three trials. [c] Yields of NH_3 and N_2H_4 were determined by ^{1}H NMR measurement and *p*-dimethylaminobenzaldehyde methods, respectively. [complex]: 1.19 × 10^{-2} M for this work.

One is that there is a significant difference in the yield ratio of ammonia to hydrazine between the current Cr complexes containing [$\mathbf{L^{Pen}}$]$^{3-}$ or [$\mathbf{L^{Cy}}$]$^{3-}$ and the previous Cr complexes containing [$\mathbf{L^{Bn}}$]$^{3-}$. That is, the yield of ammonia was significantly higher in the previous study than in this one [71]. The major difference between these two systems is that the carbon at the substituent-binding site of triamidoamine ligands [$\mathbf{L^{Pen}}$]$^{3-}$ and [$\mathbf{L^{Cy}}$]$^{3-}$ is a tertiary carbon, whereas the carbon in ligand [$\mathbf{L^{Bn}}$]$^{3-}$ is a secondary carbon. The former is densely packed, while the latter is not so much. Here, let's trace the dinitrogen reduction reaction catalyzed by Cr complexes. First, the Cr(III) complexes bind with dinitrogen molecules to form chromium(IV) dinitrogen complexes. Next, under N_2 atmosphere, when the dinitrogen molecule bound to chromium atom is reduced by K[$C_{10}H_8$], an intermediate is formed in which the generated K^+ ions interact with the dinitrogen ligand. Subsequently, protons are supplied to this intermediate, yielding ammonia and/or hydrazine. That is, if the reduction of the coordinated dinitrogen ligands is complete, ammonia is formed, however, if it is incomplete, hydrazine is produced. At this time, potassium, which binds to the coordinated dinitrogen in side-on mode, is considered more effective in cleaving the N-N bond. Consequently, ligands that promote the formation of more spatially sparse chromium complexes are considered advantageous for ammonia production. The Cr complexes coordinated with [$\mathbf{L^{Pen}}$]$^{3-}$ or [$\mathbf{L^{Cy}}$]$^{3-}$ result in more densely packed dinitrogen chromium complexes than those with [$\mathbf{L^{Bn}}$]$^{3-}$. This likely prevented the supply of protons and potassium ions after dinitrogen reduction, thereby preventing ammonia formation.

 doi:10.20944/preprints202512.1439.v1

Another is that complex **5(THF)** exhibited the highest yield of hydrazine among complexes **1** – **6**. Complex **4** also produced hydrazine in a reasonably large yield, though not as high as **5(THF)**. This is understandable considering that complex **4** is a precursor into **5(THF)**. The high yield of hydrazine in complexes **4** and **5(THF)** is plausible base on the preceding explanation. Specifically, the Cr complex bearing the $[\mathbf{L}^{Cy}]^{3-}$ ligand, which is sterically bulkier than $[\mathbf{L}^{Pen}]^{3-}$, adopts a highly hindered structure. This prevents the formation of a dinuclear Cr complex, resulting instead in the mononuclear complex **4**. Due to this highly hindered structure, even when dinitrogen binds to chromium ions, it forms structure such as **5(THF)** without forming dinuclear chromium complexes, where dinitrogen bridges between Cr and K^+. Furthermore, the sterically hindered structure of complex **5** prevents K^+ ions from interacting sufficiently with the dinitrogen from the side. As a result, the dinitrogen cannot be sufficiently activated, leading to hydrazine production. The previously reported Cr complex containing $[\mathbf{L}^{Bn}]^{3-}$ produced ammonia as the main product, despite having a structure similar to **5(THF)**. This is attributed to its spatially more open structure.

To clarify whether the above interpretations are correct, we tracked the reaction intermediates formed when **1**, **3**, **4**, and **6** reacted with a reducing agent in THF and C_6D_6 solutions using IR and ^1H NMR spectroscopy (Figures S20–S27). Note that $K[C_{10}H_8]$ is unsuitable for IR spectroscopy in this study, therefore K metal was used as the reducing agent. First, when complexes **1** and **4**, bearing $[\mathbf{L}^{Pen}]^{3-}$ and $[\mathbf{L}^{Cy}]^{3-}$ ligands respectively, were reacted with K metal under N_2 atmosphere, new IR active peaks appeared at 1805, 1746, and 1582 cm^{-1} for complex **1** (Figure S20) and at 1801 and 1576 cm^{-1} for complex **4** (Figure S22), respectively. The peak at 1805 cm^{-1} detected in the reaction with **1** corresponded to the $\nu(^{14}N–^{14}N)$ stretching vibration peak (1805 cm^{-1}) of complex **2** measured in THF (spectra B and C in Figure S20). The IR peak at 1801 cm^{-1} detected in the reaction with complex **4** ($\nu(^{15}N\text{-}^{15}N)$: 1743 cm^{-1}) was close to the peak of **5(THF)** measured in THF (1809 cm^{-1}) (spectra B and D in Figure S22). The minor peak at 1746 cm^{-1} (spectrum B in Figure S20) detected in the reaction with complex **1** closely resembled the IR peak (1743 cm^{-1}) (spectrum A in Figure S2) of complex **2** measured in the solid state. These findings suggest that complexes **1** and **4** react with K metal under N_2 atmosphere to adopt structures similar to those seen in the crystal structures of complexes **2** (Figure 1) and **5(THF)** (Figure 5). This means that the dinitrogen ligand coordinated to the chromium ion interacts with the potassium ion *via* a side-on mode and/or an end-on mode, similar to their crystal structures.

Regarding the broad peaks appearing around 1582 and 1576 cm^{-1} after the reduction reactions of complexes **1** (Figure S20) and **4** (Figure S22), respectively, the small peaks observed at approximately the same positions in the solid-state IR spectra of complexes **2** and **5(THF)**, at 1576 and 1593 cm^{-1} respectively, did not shift even when ^{15}N-labeled N_2 was used (Fig. S2 and S3), suggesting that these peaks are unrelated to the dinitrogen ligand.

Furthermore, when reacting **1** or **4** with metal K, the ^1H NMR peaks for complex **1**, except for the Et_2O peak, matched those of **2**, the ^1H NMR peaks for **4** could not be assigned due to its paramagnetism (Figures S21 and S23). These results indicate that complex **4**, possessing sterically hindered groups, generates only compounds that the dinitrogen binds to the chromium ion and potassium ion in a bridging fashion during the reaction of the complex **4** with K metal under N_2 atmosphere. On the other hand, complex **1**, which possesses a low-stereochemically barrier ligand $[\mathbf{L}^{Pen}]^{3-}$, appears to generate not only such compounds but also a small amount of compounds where the dinitrogen ligand bridges a chromium ion and two potassium ions in end-on and side-on modes.

In addition, IR spectra of the solutions obtained by the reactions of Cr(IV) complexes **3** and **6** with K metal in THF under N_2 atmosphere revealed new peaks at 1806 and 1801 cm^{-1}, respectively, which are considered to originate from the ν(N–N) stretching vibrations (Figures S24 and S26). The former peak at 1806 cm^{-1} obtained in the reaction of **3** closely matched that of complex **2** (1805 cm^{-1}) measured in THF (Figure S5 and spectrum D in Figure 24) and also that (1805 cm^{-1}) obtained after reacting complex **1** with K metal in THF (Figure S20 and spectrum C in Figure 24). The latter peak at 1801 cm^{-1} obtained in the reaction of **6** matched the peak of the species obtained after reacting complex **4** with K metal in THF (spectra B and C in Figure S26).

 doi:10.20944/preprints202512.1439.v1

Furthermore, the ^{1}H NMR spectra of complex solutions of **3** and **6** reacting with metallic potassium under N_2 atmosphere were investigated. The ^{1}H NMR spectrum obtained after the reaction of **3** with K metal (Figure S25) was consistent with the spectrum of **2** in THF solution and also agreed well with the spectrum obtained after the reaction of **1** with K metal (Figure S21). The latter spectrum (Figure S27) after the reaction of **6** with K metal resembled that of **5(THF)** in C_6D_6 (Figure S18), although it could not be identified. Therefore, it is considered that complexes **3** and **6** also formed species similar to the structures of **2** and **5(THF)**, respectively, when reacted with K metal under N_2 atmosphere. The findings regarding the formation behavior of intermediates in the reduction reaction of Cr complexes in solution well reflect the two aforementioned explanations concerning nitrogen fixation.

3. Materials and Methods

3.1. General Procedures

All manipulations were carried out under an inert atmosphere (N_2 or Ar) using either a vacuum/gas manifold or an MBraun MB 150-G glovebox. Reagents and solvents employed were commercially available. All anhydrous solvents were purchased from Kanto Chemical Co., Inc. The ligands, tris(2-(3-pentylamino)ethyl)amine (**H$_3$L^{Pen}**) and tris(2-dicyclohexylmethylaminoethyl)amine (**H$_3$L^{Cy2}**), were synthesized according to the literature methods [72]. Complex **3**, [CrCl(**L^{Pen}**)], was synthesized according to the literature method [71].

3.2. Physical Measurements

^{1}H and ^{13}C NMR spectra were recorded on a JEOL JNM-ECA500 FT NMR spectrometer (500 MHz (^{1}H), 125.77 MHz (^{13}C)), and ^{15}N NMR spectra were recorded on a JNM-ECA600 FT NMR spectrometer (60.815 MHz (^{15}N)). All NMR spectra were acquired in C_6D_6 or DMSO-d_6 at 298 K. ^{1}H and ^{13}C chemical shifts were referenced using residual protonated solvent resonances (C_6D_6: 7.16 ppm (^{1}H) and 128.06 ppm (^{13}C), DMSO-d_6: 2.50 ppm (^{1}H)). ^{15}N chemical shifts were externally referenced to $HCONH_2$ (–266.712 ppm (^{15}N)). FT IR spectra were recorded on an Agilent Cary 630 FT IR spectrophotometer. The IR spectra of the crystals were recorded using the ATR method, while those for the solution were recorded by the transmission method using a CaF_2 cell. Elemental analyses were recorded on a Perkin Elmer CHN–900 elemental analyzer. The effective magnetic moments (μ_{eff}) of solution samples of **1**, **4** and **6** were calculated from solution magnetic susceptibility data, which were determined based on the chemical shift of the methyl proton in toluene (Evans method) [75,76]. Resonance Raman spectroscopy was performed using a JASCO NRS–5500 spectrometer with 532 nm laser as excitation source, and the Raman shifts were calibrated using a Si plate (520 cm^{-1}).

3.3. X-ray Crystallography Procedures

The X-ray diffraction data for complexes **1**, **2**, **4**, **5(THF)**, **5′** and **6** were collected on a Rigaku R-AXIS RAPID II diffractometer using multi-layer mirror-monochromatized Cu$K\alpha$ (λ = 1.54178 Å) radiation. Crystallographic data and experimental details are summarized in Table S1. The calculations were performed with the Olex2 software package [77]. All structures were solved by intrinsic phasing using the ShelXT program [78], and the remaining non-hydrogen atoms were located from subsequent difference Fourier maps. The structures were refined on F^2 using full-matrix least-squares minimization with ShelXL [79]. All non-hydrogen atoms were refined anisotropically, unless otherwise stated. Hydrogen atoms were placed at idealized positions and refined using a riding model, unless otherwise stated. Complex **5'** was obtained from the sample vial during the ^{15}N-NMR measurement of the sample obtained under $^{15}N_2$ atmosphere. Therefore, complex **5'** contains $^{15}N_2$, but it should be noted that the structural refinement in its crystal structure analysis was performed assuming these atoms as ^{14}N atoms (Tables S1, S3, Figure S7). CCDC-2502967 (**1**), 2502968 (**2**), 2218004 (**3**), 2502969 (**4**), 2502970 (**5(THF)**), 2504580 (**5′**), 2502971 (**6**) contain the supplementary crystallographic data for this paper. These data can be obtained free of charge *via*

 doi:10.20944/preprints202512.1439.v1

www.ccdc.acm.ac.jk/data_request/cif, or by contacting The Cambridge Crystallographic Data Centre, 12 Union Road, Cambridge CB2 1EZ, UK; fax: +44 1223 336033.

3.4. Synthesis of [{Cr(L^{pen})}$_2$(μ-^{14}N$_2$)] (1)

A 20 mL Schlenk flask was charged with **H$_3$L^{Pen}** (1.0 g, 2.8 mmol) and Et$_2$O (4 mL) and cooled to –60 °C under ^{14}N$_2$ atmosphere, to which *n*-butyllithium (3.2 mL, 8.4 mmol, 2.6 M in hexane) was added *via* syringe. After 15 min, the reaction mixture was slowly warmed to 25 °C and was stirred for 1 h at room temperature. The reaction mixture was then cooled to –60 °C, and the resulting suspension was transferred *via* cannula to another Schlenk flask containing CrCl$_3$ (0.44 g, 2.8 mmol). The reaction mixture was again slowly warmed to 25 °C and was stirred overnight. The solvent was removed in vacuo, and the residue was extracted with Et$_2$O (6 mL). The extract was filtered through Celite. The Et$_2$O extract was transferred to a 20 mL Schlenk flask and stored in a freezer at –35 °C. [{Cr(**L^{pen}**)}$_2$(μ-^{14}N$_2$)] was obtained as dark red crystals, which were washed with acetone and dried in vacuo (yield 0.56 g, 48 %). ^{1}H NMR (500 MHz, C$_6$D$_6$, 298 K): δ(ppm) 12.14, 5.00, 0.79, –38.3. FT IR (ATR, cm^{-1}): 2956, 2924, 2898, 2870, 2851, 2822, 2797, 1446, 1370, 1349, 1340, 1329, 1277, 1260, 1237, 1208, 1163, 1148, 1128, 1111, 1085, 1047, 1025, 1016, 997, 954, 904, 895, 861, 835, 814, 800, 755, 744, 652, 613, 598, 561, 533, 524, 477. Anal. Calcd. for C$_{42}$H$_{90}$Cr$_2$N$_{10}$•1.25H$_2$O: C, 58.53; H, 10.82; N, 16.26. Found: C, 58.51; H, 10.81; N, 16.17. μ_{eff} = 2.87 μ_B (Evans method).

3.5. Synthesis of [{Cr(L^{pen})}$_2$(μ-^{15}N$_2$)] (1′)

^{15}N-labeled dinitrogen complex **1** (**1′**) was prepared following the same procedure described for complex **1**, using ^{15}N$_2$ instead of ^{14}N$_2$. Complex **1′** was obtained as dark red crystals (yield 0.37 g, 31 %). FT IR (ATR, cm^{-1}): 641 (ν(Cr–^{15}N)).

3.6. Synthesis of [{CrK(L^{pen})(μ-^{14}N$_2$)(Et$_2$O)}$_2$] (2)

A 10 mL vial was charged with complex **1** (500 mg, 0.60 mmol) and Et$_2$O (2.0 mL) under ^{14}N$_2$. Then, potassium metal (235 mg, 6.0 mmol, 10 equiv.) was added, and the mixture was stirred vigorously at room temperature overnight. The reaction mixture was filtered through Celite, and the filtrate was stored in the freezer at –30 °C to afford dark green crystals. The crystals were collected, washed with hexane, and dried in vacuo (yield 473 mg, 72 %). This compound decomposes quickly upon exposure to air, making it impossible to measure elemental analysis. ^{1}H NMR (500 MHz, C$_6$D$_6$, 298 K): δ(ppm) = 1.12 (*t*, 12H, C*H*$_{3-Et2O}$), 1.26 (*t*, 36H, CHCH$_2$–C*H*$_3$), 1.65 (*t*, 12H, –C*H*$_{2-tren}$), 1.87 (*m*, CHC*H*$_2$–C*H*$_3$), 1.93 (*m*, 12H, CHC*H*$_2$–C*H*$_3$), 3.27 (*t*, 8H, –C*H*$_{2-Et2O}$), 3.34 (*t*, 12H, –C*H*$_{2-tren}$), 4.31 (*m*, 6H, –C*H*CH$_2$CH$_3$). ^{13}C{^{1}H} NMR (125.77 MHz, C$_6$D$_6$, 298 K): δ(ppm) = 68.18, 51.93, 51.30, 29.36, 13.39. FT-IR (ATR, cm^{-1}): 2956, 2922, 2848, 2797, 2654, 1787, 1743, 1576, 1457, 1448, 1442, 1372, 1340, 1331, 1314, 1299, 1280, 1260, 1237, 1206, 1148, 1128, 1100, 1081, 1044, 1025, 995, 947, 908, 894, 863, 829, 796, 755, 595, 559, 537, 522, 479, 444.

3.7. Synthesis of [{CrK(L^{pen})(μ-^{15}N$_2$)(Et$_2$O)}$_2$] (2′)

^{15}N-labeled dinitrogen complex **2** (**2′**) was prepared following the same procedure described for complex **2**, using ^{15}N$_2$ instead of ^{14}N$_2$. Complex **2′** was obtained as dark green crystals (yield 427 mg, 65%). ^{15}N NMR (60.815 MHz, C$_6$D$_6$, 298 K): δ(ppm) = –1.9 (N$_\alpha$), –32 (N$_\beta$). FT IR (ATR, cm^{-1}): 1728, 1687 (ν(^{15}N–^{15}N)).

3.8. Synthesis of [Cr(L^{Cy})] (4)

Complex **4** was prepared following the same procedure described for complex **1**, using **H$_3$L^{Cy}** instead of **H$_3$L^{pen}**. Additionally, THF was used as the reaction solvent, and hexane was used for recrystallization, in place of Et$_2$O (yield 301 mg, 28 %). ^{1}H NMR (500 MHz, C$_6$D$_6$, 298 K): δ(ppm) = 2.8, 2.6, 2.3, 2.1, 1.9, 1.8, 1.7, 1.5, 1.3, 0.9, 0.3, –18, –35, –66. FT IR (ATR, cm^{-1}): 2954, 2919, 2874, 2848, 2796, 1603, 1528, 1446, 1377, 1347, 1325, 1305, 1280, 1258, 1234, 1208, 1144, 1131, 1096, 1072, 1031, 999, 967, 952, 891, 850, 833, 788, 781, 764, 725, 708, 691, 621, 602, 567, 485, 449. Anal. Calcd. for

 doi:10.20944/preprints202512.1439.v1

$C_{45}H_{81}CrN_4$•0.5(H_2O): C, 73.12; H, 11.18; N, 7.58. Found: C, 73.33; H, 11.47; N, 7.51. μ_{eff} = 3.82 μ_B (Evans method).

3.9. Synthesis of [CrK(L^{Cy})(μ-$^{14}N_2$)(18-crown-6)(THF)] (5(THF))

A 15 mL vial was charged with complex **4** (0.20 g, 0.27 mmol) and THF (4 mL) under $^{14}N_2$ atmosphere. Potassium metal (0.11 g, 2.7 mmol, 10 equiv.) was added, and the resulting mixture was stirred at R.T. for overnight. The mixture solution was filtered through Celite. A solution of 18-crown-6-ether (79.3 mg, 0.30 mmol) in THF (1 mL) was added to the filtrate, and the mixture was stirred at R.T. for 1 min. Hexane (6 mL) was slowly added to the reaction mixture. The solution was allowed to stand at –35 °C to give complex **5** as green crystals (172 mg, 51 %). This compound decomposes quickly on exposure to air, making it impossible to measure elemental analysis. ^{1}H NMR (500 MHz, C_6D_6, 298 K): δ(ppm) = 4.58 (*br*, 3H, N–C*H*–Cy), 3.62 (*br*, 6H, –CH_2–$_{Cy}$), 3.58 (*t*, 4H, O–CH_2–$_{THF}$), 3.53 (*br*, 12H, –CH_2–$_{18\text{-crown-6-ether}}$), 3.20 (*br*, 12H, –C$H_2$–$_{18\text{-crown-6-ether}}$), 2.38 (*t*, 12H, –C$H_2$–$_{tren}$), 2.10 – 1.10 (*m*, 66H, –CH_2–$_{Cy}$, –CH_2–$_{n\text{-hexane}}$),1.42 (*m*, 4H, –CH_2–$_{THF}$). FT IR (ATR, cm^{-1}): 2911, 2844, 2745, 1824, 1465, 1444, 1364, 1349, 1334, 1327, 1284, 1256, 1249, 1236, 1219, 1193, 1178, 1141, 1131, 1113, 1105, 1068, 1040, 1016, 997, 962, 909, 891, 874, 839, 827, 800, 786, 775, 753, 727, 704, 695, 626, 615, 596, 578, 550, 533, 488, 447, 440, 432, 440, 432, 432.

3.10. Synthesis of [CrK(L^{Cy})(μ-$^{15}N_2$)(18-crown-6)(THF)] (5′(THF))

^{15}N-labeled dinitrogen complex **5(THF)** (**5′(THF)**) was prepared following the same procedure described for complex **5**, using $^{15}N_2$ instead of $^{14}N_2$. Complex **5′(THF)** was obtained as green crystals (yield 74.2 mg, 22 %). ^{15}N NMR (60.815 MHz, C_6D_6, 298 K): δ(ppm) = 8.8 (N_α), –27.5 (N_β). FT IR (ATR, cm^{-1}): 1757 (ν(^{15}N–^{15}N)).

3.11. Synthesis of [CrK(L^{Cy})(μ-$^{14}N_2$)(18-crown-6)] (5)

Complex **5** was obtained as a green, THF-free crystal by leaving a C_6D_6 solution of **5(THF)** in a NMR sample tube at room temperature for several days (yield 10 %). ^{1}H NMR (500 MHz, C_6D_6, 298 K): δ(ppm) = 4.58 (*br*, 3H, Cy–C*H*–Cy), 3.62 (*br*, 6H, –CH_2–$_{tren}$), 3.53 (*br*, 12H, –CH_2–$_{Cy}$), 3.21 (*br*, 24H, –CH_2–$_{18\text{-crown-6-ether}}$), 2.39 (*br*, 18H, –C$H_2$–$_{Cy}$), 2.10 – 1.10 (*m*, 66H, –CH_2–$_{Cy}$, –CH_2–$_{tren}$, –CH_2–$_{n\text{-hexane}}$). FT IR (ATR, cm^{-1}): 1813 (ν(^{14}N–^{14}N)).

3.12. Synthesis of [CrK(L^{Cy})(μ-$^{15}N_2$)(18-crown-6)] (5′)

^{15}N-labeled dinitrogen complex **5** (**5′**) was obtained as a green crystal by leaving the C_6D_6 solution of **5′** in a NMR sample tube at room temperature for several days (yield 9.5 %). ^{15}N NMR (60.815 MHz, C_6D_6, 298 K): δ (ppm) = 8.8 (N_α), –27.5 (N_β). FT IR (ATR, cm^{-1}): 1753 (ν(^{15}N–^{15}N)).

3.13. Synthesis of [CrCl(L^{Cy})] (6)

Complex **6** was synthesized by the literature method using [$\mathbf{L}^{Cy}$]$^{3-}$ instead of [($Me_3SiNCH_2CH_2$)$_3$N]$^{3-}$ and recrystallized from cyclopentylmethylether solution of **6** in cyclopentylmethylether (yield 39 %) [74]. ^{1}H NMR (500 MHz, C_6D_6, 298 K): δ(ppm) = 13, 3.6, 3.1, 1.7, 1.5, 1.4, 1.1, -41.0. FT IR (ATR, cm^{-1}): 2915, 2846, 2818, 1608, 1446, 1351, 1325, 1293, 1280, 1258, 1234, 1221, 1210, 1193, 1183, 1142, 1129, 1088, 1073, 1027, 1016, 967, 952, 936, 921, 893, 865, 852, 833, 800, 786, 755, 704, 626, 600, 580, 565, 546, 518, 483. Anal. Calcd. for $C_{45}H_{81}ClCrN_4$•1.25($C_6H_{12}O$): C, 70.78; H, 10.86; N, 6.29. Found: C, 70.81; H, 11.13; N, 6.37. μ_{eff} = 2.96 μ_B (Evans method).

3.14. Reactions of 1, 2, 3, 4, 5(THF), and 6 with K[$C_{10}H_8$] and HOTf

A 5 mL THF solution of the reducing agent (K[$C_{10}H_8$]) freshly prepared from metallic potassium (5.6 mg, 0.14 mmol, 12 eq.) and naphthalene (18 mg, 0.14 mmol, 12 equiv.) in a 20 mL Schlenk flask was added to a 5 mL THF solution of each chromium complex (5.95 × 10^{-2} mmol) at –78 °C, and the mixture was stirred for 1 h under N_2. HOTf (trifluoromethanesulfonic acid, 42 mg, 0.28 mmol) was added to reaction mixture of chromium complex under vigorous stirring, and the resultant solution

 doi:10.20944/preprints202512.1439.v1

was slowly warmed to 25 °C. After the solution was stirring for 1 h at room temperature, the solvents were removed under reduced pressure to give a white solid containing ammonium and hydrazinium salts. The residue in the Schlenk tube was washed with diethyl ether and then extracted with H_2O (5 mL). The aqueous extract was evaporated, and the residue was analyzed using ^1H NMR spectroscopy (for NH_3) or *p*-dimethylaminobenzaldehyde method (for N_2H_4).

3.15. NH_3 Quantification Procedure

Ammonium salts were quantified using ^1H NMR spectroscopy. The quantification of NH_4^+ was carried out using the method reported by Ashley and coworkers [80]. The $14NH_4^+$ resonance was integrated using the vinyl proton of 2,5-dimethylfuran in DMSO-d_6 sealed in the capillary as the reference (*d*: 5.83, s, 2H). This quantification was calibrated using a standard 2.6×10^{-2} M solution of NH_4^+ in DMSO-d_6 (Figure S26 and Table S4).

3.16. N_2H_4 Quantification Procedure

The quantification of $N_2H_6^{2+}$ was carried out using the method reported by Ashley and coworkers [80]. The residues were dissolved in H_2O (10 mL), and the resulting solution was diluted tenfold with H_2O. Aliquots of the diluted solution were analyzed for N_2H_4 *via* UV-vis spectroscopy using a standard spectrophotometric method. This involved reacting the sample with an acidic *p*-dimethylaminobenzaldehyde solution and generating a yellow azine dye with a characteristic absorption maximum (λ_{max}) at 458 nm. The N_2H_4 content in the aliquot was quantified by comparison to the calibration curve (Figure S27).

4. Conclusions

In this study, six chromium complexes with the triamidoamine derivative ligand bearing bulky substituents at their terminal positions, $[\mathbf{L}^{Pen}]^{3-}$ or $[\mathbf{L}^{Cy}]^{3-}$, were synthesized and structurally characterized. Using these chromium complexes, the effect of the ligand substituents on the nitrogen fixation reactivity was investigated. When employing chromium complex bearing slightly less bulky ligand $[\mathbf{L}^{Pen}]^{3-}$, the dinitrogen dichromium complex, Cr(IV)-N_2-Cr(IV) (**1**), was prepared under N_2 atmosphere. And further reduction of this complex with reductant K metal under N_2 atmosphere yielded the dinitrogen tetranuclear Cr_2K_2 complex, Cr(K)-(μ-N_2)$_2$-KCr (**2**). On the other hand, when the chromium complexes bearing more bulky ligand $[\mathbf{L}^{Cy}]^{3-}$ was employed, the steric hindrance prevented the formation of dichromium dinitrogen complexes, unlike that obtained with chromium complexes bearing the $[\mathbf{L}^{Pen}]^{3-}$ ligand. Instead, an axially vacant Cr(III) complex **4** was obtained. However, interestingly, when complex **4** was reduced with K metal in the presence of 18-crown-6 ether under N_2 atmosphere, a dinuclear Cr(IV)-N_2-K(18-crown-6 ether)(THF) complex (**5(THF)**) was obtained. This formation is attributable to the sterically smaller ligand of the 18-crown 6-ether. The formations of dinitrogen chromium complexes **1**, **2** and **5(THF)** were also confirmed by Raman and IR spectroscopy. The Cr(IV)Cl complexes **3** and **6**, each possessing $[\mathbf{L}^{Pen}]^{3-}$ and $[\mathbf{L}^{Cy}]^{3-}$, respectively, and lacking N_2, were also synthesized and structurally characterized to study the nitrogen fixation reactivity.

For chromium complexes **2** and **5(THF)** with ^{15}N-labeled N_2 (**2′** and **5′(THF)**), ^{15}N NMR and solution IR spectroscopic measurements were performed, revealing that the potassium ions, which coordinated in both side-on and end-on modes seen in the crystal of **2**, gradually transitioned to coordination exclusively in the end-on mode in solution. Furthermore, the results obtained from the ^{15}N NMR spectrum of **5′(THF)** revealed that the THF ligand is removed from complex **5(THF)** in solution, leading to the formation of complex **5**. Using single crystals accidentally obtained from the NMR sample tube, X-ray structural analysis was performed to yield complex **5** without THF, confirming the structure as predicted in solution.

When complexes **1** and **3** bearing the $[\mathbf{L}^{Pen}]^{3-}$ ligand reacted with potassium in solution under N_2 atmosphere, substances exhibiting IR and ^1H NMR spectra similar to those of complex **2** were

 doi:10.20944/preprints202512.1439.v1

obtained. Furthermore, the spectra obtained when complexes **4** and **6**, bearing the $[\mathbf{L}^{\mathbf{Cy}}]^{3-}$ ligand, reacted with metallic K under N_2 atmosphere were also similar to those of **5(THF)**.

Finally, nitrogen fixation reactivity was studied using complexes **1**, **2**, **3**, **4**, **5(THF)**, and **6** under N_2, employing $K[C_{10}H_8]$ as a reductant and HOTf as a proton source. The results showed that hydrazine and small amounts of ammonia were obtained in all cases. However, unlike the nitrogen fixation reaction previously reported using Cr complexes with $[\mathbf{L}^{\mathbf{Bn}}]^{3-}$ ligand [71], the ammonia yield decreased in all cases compared to the previous study [71]. And the Cr complexes **4** and **5**, which possess the bulky ligand $[\mathbf{L}^{\mathbf{Cy}}]^{3-}$, generated significantly more hydrazine than the others. These results are likely due to the fact that while the $[\mathbf{L}^{\mathbf{Pen}}]^{3-}$ and $[\mathbf{L}^{\mathbf{Cy}}]^{3-}$ ligands used in this study possess tertiary carbons, $[\mathbf{L}^{\mathbf{Bn}}]^{3-}$ has a secondary carbon. This is thought to arise from the steric hinderance of the $[\mathbf{L}^{\mathbf{Pen}}]^{3-}$ and $[\mathbf{L}^{\mathbf{Cy}}]^{3-}$ ligands inhibiting the supply of K^+ and protons. The findings obtained in this study indicate that when Cr complexes of triamidoamine ligands bearing bulky substituents react with N_2 in the presence of K, the resulting dinitrogen chromium complexes are influenced by K bound *via* ligand-dependent interaction modes. The results obtained here will provide important insights into dinitrogen activation and nitrogen fixation using chromium complexes, which have been scarcely reported to date.

Supplementary Materials: The following supporting information can be downloaded at: https://www.mdpi.com/article/doi/s1, Table S1: Experimental data for X-ray diffraction studies on crystalline complexes **1**, **2**, **4**, **5(THF)**, **5′**, and **6**; Table S2: Selected bond lengths (Å) and angles (deg) of **4**; Figure S1: Raman spectra of **1** and ^{15}N labeled **1** (**1′**) in toluene (λ_{ex} = 532 nm) at room temperature; Figure S2: IR spectra of **2** and ^{15}N labeled **2** (**2′**) (ATR); Figure S3: IR spectra of **5(THF)** and ^{15}N labeled-dinitrogen complex **5(THF)** (**5′(THF)**) (ATR); Figure S4: IR spectra of **2** in toluene, solvent toluene, and the difference; Figure S5: IR spectra of **2** in THF, solvent THF, and the difference; Figure S6: IR spectra of **5(THF)** in toluene, solvent toluene, and the difference; Figure S7: IR spectra of **5(THF)** in THF, solvent THF, and the difference; Figure S8: ^{15}N NMR spectrum of ^{15}N labeled-dinitrogen complex **2** (**2′**) in C_6D_6 (60.815 MHz); Figure S9: ^{15}N NMR spectrum of ^{15}N labeled-dinitrogen complex **5(THF)** (**5′(THF)**) in C_6D_6 (60.815 MHz); Figure S10: ^{15}N NMR spectra of ^{15}N labeled-dinitrogen complex **2** (**2′**) after 10,000, 20,000, 30,000, 40,000, and 50,000 scans in C_6D_6 (60.815 MHz); Figure S11: ORTEP view of **5′** with the atom numbering scheme (50 % probability thermal ellipsoids); Table S3: selected bond lengths (Å) and angles (deg) of **5′**; Figure S12: IR spectra of **5** and ^{15}N labeled-dinitrogen complex **5** (**5′**) (ATR); Figure S13: ^1H NMR spectra of **5** in C_6D_6 (500 MHz); Figure S14: ^1H NMR spectrum of **1** in C_6D_6 (500 MHz); Figure S15: ^1H NMR spectra of **2** in C_6D_6 (500 MHz); Figure S16: ^1H NMR spectra of **3** in C_6D_6 (500 MHz); Figure S17: ^1H NMR spectra of **4** in C_6D_6 (500 MHz); Figure S18: ^1H NMR spectra of **5(THF)** in C_6D_6 (500 MHz); Figure S19: ^1H NMR spectra of **6** in C_6D_6 (500 MHz); Figure S20: IR spectra of **1** in THF, **1** with K metal in THF under $^{14}N_2$, and **2** in THF; Figure S21: ^1H NMR spectra of **2** in C_6D_6 and **1** with K metal in C_6D_6 under N_2 (500 MHz); Figure S22: IR spectra of **4** in THF, **4** with K metal in THF under $^{14}N_2$, **4** with K metal in THF under $^{15}N_2$, and **5(THF)** in THF; Figure S23: ^1H NMR spectra of **4** with K metal under N_2 in C_6D_6 (500 MHz); Figure S24: IR spectra of **3** in THF under $^{14}N_2$, **3** with K metal in THF under $^{14}N_2$, **1** with K metal in THF under $^{14}N_2$, **2** in THF, and THF; Figure S25: ^1H NMR spectra of **2** in C_6D_6 and **3** with K metal in C_6D_6 under $^{14}N_2$; Figure S26: IR spectra of **6** in THF under $^{14}N_2$, **6** with K metal in THF under $^{14}N_2$, **4** with K metal in THF under $^{14}N_2$, **5(THF)** in THF, and THF; Figure S27: ^1H NMR spectra of **6** with K metal in C_6D_6 under $^{14}N_2$; Table S4: yields of NH_3 and N_2H_4 from the reaction of complexes **1**, **2**, **3**, **4**, **5(THF)**, and **6** with $K[C_{10}H_8]$ and an HOTf; Figure S28: ^1H NMR spectrum of $^{14}NH_4^+$ that was obtained from the reaction of **1** with 12 equiv. $K[C_{10}H_8]$ and 12 equiv. HOTf under $^{14}N_2$ (DMSO-d_6, 500 MHz); Figure S29: Calibration curves for hydrazine quantification.

Author Contributions: Conceptualization, T.K., Y.K., Y.K.*; methodology, T.K., Y.K., Y.K.*; validation, T.K., Y.K., Y.K.*; formal analysis, T.K., Y.K., Y.K.*, H.N., T.F., T.O.; investigation, T.K., Y.K., Y.K.*; data curation, T.K., Y.K.; writing—original draft preparation, T.K., Y.K., Y.K.*; writing—review and editing, Y.K.*, H.M.; supervision, Y.K.*, H.M.; project administration, Y.K.*; funding acquisition, Y.K., Y.K.*, H.M.

Funding: This research was funded by the Japan Society for the Promotion of Science (JSPS), grant number 24K217860 and the Nitto Foundation.

 doi:10.20944/preprints202512.1439.v1

Institutional Review Board Statement: Not applicable.

Informed Consent Statement: Not applicable.

Acknowledgments: We thank Ms. Haruyo Nagao (Institute for Molecular Science) for ^{15}N NMR spectroscopy measurement. This work was conducted in Institute for Molecular Science, supported by Advanced Research Infrastructure for Materials and Nanotechnology in Japan (ARIM)" of the Ministry of Education, Culture, Sports, Science and Technology (MEXT). Proposal Number JPMXP1225MS1082. We also acknowledge the Japan Society for the Promotion of Science (JSPS) for a Grant-in Aid for Challenging Research Exploratory Research (24K21786) and the Nitto Foundation..

Conflicts of Interest: The authors declare no conflict of interest.

Abbreviations

The following abbreviations are used in this manuscript:

THF	Tetrahydrofuran
HOTf	Trifluoromethanesilfonic Acid
IR	Infrared
tren	Tris(2-aminoethyl)amine
n-BuLi	*n*-Butyllithium
Et_2O	Diethylether
ORTEP	Oak Ridge Thermal-Ellipsoid Plot
NMR	Nuclear Magnetic Resonance

References

1. Schlögl, R. Catalytic Synthesis of Ammonia–A "Never-Ending Story"? *Angew. Chem. Ent. Ed.* **2003**, *42*, 2004–2008.
2. Zhang, X.; Ward, B. B.; Sigman, D. M. Global Nitrogen Cycle: Critical Enzymes, Organisms, and Processes for Nitrogen Budgets and Dynamics. *Chem. Rev.* **2020**, *120*, 5308–5351.
3. Elishav, O.; Lis, B. M.; Miller, E. M.; Arent, D. J.; Valera-Medina, A.; Dana, A. G.; Shter, G. E.; Grader, G. S. Progress and Prospective of Nitrogen-Based Alternative Fuels. *Chem. Rev*. **2020**, *120*, 5352–5436.
4. Yandulov, D. V.; Schrock, R. R. Catalytic Reduction of Dinitrogen to Ammonia at a Single Molybdenum Center. *Science* **2003**, *301*, 76–78.
5. Schrock, R. R. Catalytic Reduction of Dinitrogen to Ammonia t a Single Molybdenum Center. *Acc. Chem. Res.* **2005**, *38*, 955–962.
6. Schrock, R. R. Catalytic Reduction of Dinitrogen to Ammonia by Molybdenum: Theory versus Experiment. *Angew. Chem. Int. Ed.* **2008**, *47*, 5512–5522.
7. Mitsumoto, T.; Ashida, Y.; Arashiba, K.; Kuriyama, S.; Egi, A.; Tanaka, H.; Yoshizawa, K.; Nishibayashi, Y. Catalytic Activity of Molybdenum Complexes Bearing PNP-Type Pincer Ligand toward Ammonia Formation. *Angew. Chem. Int. Ed*. **2023**, *62*, e202306631.
8. Tanabe, Y.; Nishibayashi, Y. Catalytic Nitrogen Fixation Using Well-Defined Molecular Catalysts under Ambient or Mild Reaction Conditions. *Angew. Chem. Int. Ed.* **2024**, *63*, e202406404.
9. Mitsumoto, T.; Nakamura, T.; Tanaka, H.; Yoshizawa, K.; Nishibayashi, Y. Cooperative Ammonia Formation Catalyzed by Molybdenum and Samarium Complexes. *Angew. Chem. Int. Ed*. **2025**, *64*, e202507061.
10. Mitsumoto, T.; Nishibayashi, Y. Molybdenum-Catalyzed Ammonia Synthesis by Using Zero-Valent Metal Powder with Alcohols or Water, *Angew. Chem. Int. Ed*. **2025**, *64*, e202423858.
11. McWilliams, S. F.; Holland, P. L. Dinitrogen Binding and Cleavage by Multinuclear Iron Complexes. *Acc. Chem. Res.* **2015**, *48*, 2059–2065.
12. Tanaka, H.; Nishibayashi, Y.; Yoshizawa, K. Interplay between Theory and Experiment for Ammonia Synthesis Catalyzed by Transition Metal Complexes. *Acc. Chem. Res*. **2016**, *49*, 987–995.
13. Ashida, Y.; Nishibayashi, Y. Catalytic Conversion of Nitrogen Molecule into Ammonia Using Molybdenum Complexes under Ambient Reaction Conditions. *Chem. Commun*. **2021**, *57*, 1176–1189.

 doi:10.20944/preprints202512.1439.v1

14. Tanabe, Y.; Nishibayashi, Y. Comprehensive insights into synthetic nitrogen fixation assisted by molecular catalysts under ambient or mild conditions. *Chem. Soc. Rev.* **2021**, *50*, 5201–5242.
15. Tanabe, Y.; Nishibayashi, Y. Recent advances in catalytic silylation of dinitrogen using transition metal complexes. *Coord. Chem. Rev*. **2019**, *389*, 73–93.
16. Tanabe, Y.; Nishibayashi, Y. Recent advances in catalytic nitrogen fixation using transition metal-dinitrogen complexes under mild reaction conditions. *Coord. Chem. Rev*. **2022**, *472*, 214783.
17. Tanifuji, K.; Ohki, Y. Metal-Sulfur Compounds in N_2 Reduction and Nitrogenase-Related Chemistry. *Chem. Rev*. **2020**, *120*, 5194–5251.
18. Singh, D.; Buratto, W. R.; Torres, J. F.; Murray, L. J. Activation of Dinitrogen by Polynuclear Metal Complexes. *Chem. Rev*. **2020**, *120*, 5517–5581.
19. Chalkley, M. J.; Drover, M. W.; Peters, J. C. Catalytic N_2-to-NH_3 (or -N_2H_4) Conversion by Well-Defined Molecular Coordination Complexes. *Chem. Rev*. **2020**, *120*, 5582–5636.
20. Kim, S.; Loose, F.; Chirik, P. J. Beyond Ammonia: Nitrogen -Element Bond Forming Reactions with Coordinated Dinitrogen. *Chem. Rev*. **2020**, *120*, 5637–5681.
21. Khoenkhoen, N.; de Bruin, B.; Reek, J. N. H.; Dzik, W. I. Reactivity of Dinitrogen Bound to Mid- and Late-Transition-Metal Centers. *Eur. J. Inorg. Chem.* **2015**, 567–598.
22. Stucke, N.; Flöser, B. M.; Weyrich, T.; Tuczek, F. Catalytic Ammonia Synthesis with Transition Metal Complexes: Recent Developments. *Eur. J. Inorg. Chem*. **2017**, 1337–1355.
23. Bhutto, S. M.; Holland, P. L. Dinitrogen Activation and Functionalization Using β-Diketiminate Iron Complexes. *Eur. J. Inorg. Chem.* **2019**, 1861–1869.
24. Kendall, A. J.; Mock, M. T. Dinitrogen Activation and Functionalization with Chromium. *Eur. J. Inorg. Chem*. **2020**, 1358–1375.
25. Nishibayashi, Y. Recent Progress in Transition-Metal-Catalyzed Reduction of Molecular Dinitrogen under Ambient Reaction Conditions. *Inorg. Chem.* **2015**, *54*, 9234–9247.
26. Foster, S. L.; Perez Bakovic, S. I.; Duda, R. D.; Maheshwari, S.; Milton, R. D.; Minteer, S. D.; Janik, M. J.; Renner, J. N.; Greenlee, L. F. Catalysts for nitrogen reduction to ammonia. *Nat. Cat*. **2018,** *1*, 490–500.
27. Burford, R. J.; Fryzuk, M. D. Examining the relationship between coordination mode and reactivity of dinitrogen. *Nat. Rev. Chem.* **2017**, *1*, 0026.
28. Kuriyama, S.; Nishibayashi, Y. Development of catalytic nitrogen fixation using transition metal complexes not relevant to nitrogenases. *Tetrahedron* **2021**, *83*, 131986.
29. Kireev, N. V.; Filippov, O. A.; Epstein, L. M.; Shubina, E. S.; Belkova, N. V. Activation of dinitrogen by group 6 metal complexes. *Russ. Chem. Bull.* **2023**, *72*, 83–102.
30. Itabashi, T.; Arashiba, K.; Egi, A.; Tanaka, H.; Sugiyama, K.; Suginome, S.; Kuriyama, S.; Yoshizawa, K.; Nishibayashi, Y. Direct synthesis of cyanate anion from dinitrogen catalysed by molybdenum complexes bearing pincer-type ligand. *Nat. Commun.* **2022**, *13*, 6161.
31. Ashida, Y.; Onozuka, Y.; Arashiba, K.; Konomi, A.; Tanaka, H.; Kuriyama, S.; Yamazaki, Y.; Yoshizawa, K.; Nishibayashi, Y. Catalytic nitrogen fixation using visible light energy. *Nat. Commun*. **2022**, *13*, 7263.
32. Yamazaki, Y.; Endo, Y.; Nishibayashi, Y. Catalytic ammonia formation from dinitrogen, water, and visible light energy. *Nat. Commun*. **2025**, *16*, 4540.
33. Ashida, Y.; Mizushima, T.; Arashiba, K.; Egi, A.; Tanaka, H.; Yoshizawa, K.; Nishibayashi, Y. Catalytic production of ammonia from dinitrogen employing molybdenum complexes bearing N-heterocyclic carbene-based PCP-type pincer ligands. *Nat. Synth.* **2023**, *2*, 635–644.
34. Suginome, S.; Murota, K.; Yamamoto, A.; Yoshida, H.; Nishibayashi, Y. Mechanochemical nitrogen fixation catalysed by molybdenum complexes. *Nat. Synth.* **2025**, *4*, 243–251.
35. Suginome, S.; Nishibayashi, Y. Direct Synthesis of Organonitrogen Compounds from Dinitrogen Using Transition Metal Complexes: Leap from Stoichiometric Reactions to Catalytic Reactions. *ChemCatChem* **2023**, *15*, e202300850.
36. Eizawa, A.; Arashiba, K.; Tanaka, H.; Konomi, A.; Yoshizawa, K.; Nishibayashi, Y. Design, synthesis and reactivity of dimolybdenum complex bearing quaterphenylene-bridged pyridine-based PNP-type pincer ligand. *Dalton Trans*. **2023**, *52*, 14012–14016.

 doi:10.20944/preprints202512.1439.v1

37. Feng, D.; Zhou, L.; Liu, C.; Li, H.; Zhang, Y.; Yao, Y.; Ma, T. Enhanced electrochemical reduction of N_2 to NH_3 by interfacial engineering of biomass-derived Fe, Mo-bimetallic composite. *Electrochim. Acta* **2024**, *484*, 144096.
38. Escomel, L.; Martins, F. F.; Vendier, L.; Coffinet, A.; Queyriaux, N.; Krewald, V.; Simonneau, A. Coordination of $Al(C_6F_5)_3$ vs. $B(C_6F_5)_3$ on group 6 end-on dinitrogen complexes: chemical and structural divergences. *Chem. Sci.* **2024**, *15*, 11321–11336.
39. Zhang, G.; Li, Q.; Wang, X.; Jin, L.; Liao, Q. Diverse Behaviors of N_2 on Mo Centers Bearing POCOP-Pincer Ligands and the Role of π-Electron Configuration in Regulating the Pathway of N_2 Activation. *J. Am. Chem. Soc.* **2025**, *147*, 3747–3757.
40. Suginome, S.; Okochi, A.; Nakamura, T.; Konomi, A.; Tanaka, H.; Yoshizawa, K.; Nishibayashi, Y. Catalytic Reduction of Dinitrogen *via* Hydroboration. *J. Am. Chem. Soc.* **2025**, *147*, 26684–26692.
41. Yamazaki, Y.; Nakaya, K.; Nishibayashi, Y. Synthesis of Molybdenum Complexes Bearing Pyridine-Based PNP-Type Pincer Ligands with Pendent Pyridyl Unit and Their Catalytic Activity for Ammonia Formation. *Organometallics* **2024**, *43*, 2747–2754.
42. Mock, M. T.; Chen, S.; Rousseau, R.; O'Hagan, M. J.; Dougherty, W. G.; Scott Kassel, W.; DuBois, D. L.; Bullock, R. M. A rare terminal dinitrogen complex of chromium. *Chem. Commun*. **2011**, *47*, 12212–12214.
43. Akturk, E. A.; Yap, G. P. A.; Theopold, K. H. Mechanism-based designed of labile precursors for chromium(I) chemistry. *Chem. Commun*. **2015**, *51*, 15402–15405.
44. Egbert, J. D.; O'Hagan, M.; Wiedner, E. S.; Morris Bullock, R.; Piro, N. A.; Scott Kassel, W.; Mock, M. T. Putting chromium on the map for N_2 reduction: production of hydrazine and ammonia. A study of *cis*-$M(N_2)_2$ (M = Cr, Mo, W) bis(diphosphine) complexes. *Chem. Commun*. **2016**, *52*, 9343–9346.
45. Li, J.; Yin, J.; Wang, G.-X.; Yin, Z.-B.; Zhang, W.-X.; Xi, Z. Synthesis and reactivity of asymmetric Cr(I) dinitrogen complexes supported by cyclopentadienyl-phosphine ligands. *Chem. Commun*. **2019**, *55*, 9641–9644.
46. Duletski, O. L.; Platz, D.; Pollock, C. J.; Mosquera, M. A.; Arulsamy, N.; Mock, M. T. Dinitrogen activation at chromium by photochemically induced Cr^{II}-C bond homolysis. *Chem. Commun.* **2024**, *60*, 7029–7032.
47. Ashida, Y.; Egi, A.; Arashiba, K.; Tanaka, H.; Mitsumoto, T.; Kuriyama, S.; Yoshizawa, K.; Nishibayashi, Y. Catalytic Reduction of Dinitrogen into Ammonia and Hydrazine Using Chromium Complexes Bearing PCP-Pincer Ligand. *Chem. – Eur. J.* **2022**, *28*, e202200557.
48. Eaton, M. C.; Knight, B. J.; Catalano, V. J.; Murray, L. J. Evaluating Metal Ion Identity on Catalytic Silylation of Dinitrogen Using a Series of Trimetallic Complexes. *Eur. J. Inorg. Chem.* **2020**, 1519–1524.
49. Vidyaratne, I.; Scott, J.; Gambarotta, S.; Budzelaar, P. H. M. Dinitrogen Activation, Partial Reduction, and Formation of Coordinated Imide Promoted by a Chromium Diiminepyridine Complex. *Inorg. Chem*. **2007**, *46*, 7040–7049.
50. Berben, L. A.; Kozimor, S. A. Dinitrogen and Acetylide Complexes of Low-Valent Chromium. *Inorg. Chem*. **2008**, *47*, 4639–4647.
51. Hoffert, W. A.; Rappé, A. K.; Shores, M. P. Unusual Electronic Effects Imparted by Bridging Dinitrogen: Experimental and Theoretical Investigation. *Inorg. Chem*. **2010**, *49*, 9497–9507.
52. Mock, M. T.; Pierpont, A. W.; Egbert, J. D.; O'Hagan, M.; Chen, S.; Morris Bullock, R.; Dougherty, W. G.; Scott Kassel, W.; Rousseau, R. Protonation Studies of a Mono-Dinitrogen Complex of Chromium Supported by a 12-Membered Phosphorus Macrocycle Containing Pendant Amines. *Inorg. Chem*. **2015**, *54*, 4827–4839.
53. Salt, J. E.; Girolami, G. S.; Wilkinson, G.; Motevalli, M.; Thornton-Pett, M.; Hursthouse, M. B. Synthesis and Characterisation of 1,2-Bis(dimethylphosphino)ethane (dmpe) Complexes of Chromium-(0) and -(IV): X-Ray Crystal Structures of *trans*-$Cr(N_2)_2(dmpe)_2$, *cis*-$Cr(CO)_2(dmpe)_2$, $Cr(C_2Ph_2)_2(dmpe)$, and $CrH_4(dmpe)_2$. *J. Chem. Soc., Dalton Trans*. **1985**, 685–692.
54. Denholm, S.; Hunter, G.; Weakley, T. J. R. Dinitrogen Complexes derived from Tricarbonyl(η⁶-hexaethylbenzene)chromium(0): Crustal and Molecular Structure of μ-dinitrogen-bis[dicarbonyl(η⁶-hexaethylbenzene)chromium(0)]-Toluene (1/1). *J. Chem. Soc., Dalton Trans*. **1987**, 2789–2791.
55. Sobota, P.; Jeżowska- Trzebiatowska, B. FIXATION OF DINITROGEN AND ACETYLENE BY THE SYSTEM $CrCl_2$-Mg. ISOLATION AND PROPERTIES OF CHROMIUM COMPLEXES WITH FIXED N_2 AND C_2H_2. *J. Organomet. Chem.* **1977**, *131*, 341–345.

 doi:10.20944/preprints202512.1439.v1

56. Wang, G.-X.; Yin, Z.-B.; Wei, J.; Xi, Z. Dinitrogen Activation and Functionalization Affording Chromium Diazenido and Hydrazido Complexes. *Acc. Chem. Res.* **2023**, *56*, 3211–3222.
57. Monillas, W. H.; Yap, G. P. A.; MacAdams, L. A.; Theopold, K. H. Binding and Activation of Small Molecules by Three-Coordinate Cr(I). *J. Am. Chem. Soc.* **2007**, *129*, 8090–8091.
58. Mock, M. T.; Chen, S.; O'Hagan, M.; Rousseau, R.; Dougherty, W. G.; Scott Kassel, W.; Morris Bullock, R. Dinitrogen Reduction by a Chromium(0) Complex Supported by a 16-Membered Phosphorus Macrocycle. *J. Am. Chem. Soc.* **2013**, *135*, 11493–11496.
59. Kendall, A. J.; Johnson, S. I.; Morris Bullock, R.; Mock, M. T. Catalytic Silylation of N_2 and Synthesis of NH_3 and N_2H_4 by Net Hydrogen Atom Transfer Reactions Using a Chromium P_4 Macrocycle. *J. Am. Chem. Soc.* **2018**, *140*, 2528–2536.
60. Yin, J.; Li, J.; Wang, G.-X.; Yin, Z.-B.; Zhang, W.-X.; Xi, Z. Dinitrogen Functionalization Affording Chromium hydrazido Complex. *J. Am. Chem. Soc.* **2019**, *141*, 4241–4247.
61. Yin, Z.-B.; Wu, B.; Wang, G.-X.; Wei, J.; Xi, Z. Dinitrogen Functionalization Affording Chromium Diazenido and Side-on η^2-Hydrazido Complexes. *J. Am. Chem. Soc.* **2023**, *145*, 7065–7070.
62. Wang, G.-X.; Wang, X.; Jiang, Y.; Chen, W.; Shan, C.; Zhang, P.; Wei, J.;Ye, S.; Xi, Z. Snapshots of Early-Stage Quantitative N_2 Electrophilic Functionalization. *J. Am. Chem. Soc.* **2023**, *145*, 9746–9754.
63. Wu, B.; Chen, W.; Yan, H.; Zhang, X.; Wei, J.; Xi, Z.; Wang, G.-X.; Ye, S. Trisilylation of a Formal Cr(-I) Bis-dinitrogen Complex. *J. Am. Chem. Soc.* **2025**, *147*, 32480–32493.
64. Wang, X.; Wu, Y.; Wang, Y.; Sun, R.; Wei, J.; Xi, Z. Harnessing Chromium(V) Hydrazido Intermediates for N_2 Functionalization to Multisubstituted Hydrazines through Ligand Migration. *J. Am. Chem. Soc.* **2025**, *147*, 35413–35421.
65. Wang, X.; Wang, Y.; Wu, Y.; Wang, G.-X.; Wei, J.; Xi, Z. Syntheses and Characterizations of Hetero-Bimetallic Chromium-Dinitrogen Transition-Metal Complexes. *Inorg. Chem.* **2023**, *62*, 18641–18648.
66. Hao, M.-T.; Zhang, B.; Li, D.; Wujieti, B.; Li, X.; Chen, B.-Z. Theoretical Studies on the Reduction of N_2 to NH_3/N_2H_4 Catalyzed by Chromium Complexes. *Inorg. Chem.* **2025**, *64*, 7311–7324.
67. Li, Z.; Liu, X.-X.; Wang, X.; Peng, L.-Y.; Liu, C.; Yuan, Z.; Liu, Y.; Cui, G.; Hu, S. Catalytic Silylation of Dinitrogen by PCP-Ligated Chromium Complexes. *ACS Cat.* **2025**, *15*, 13337–13345.
68. Yin, Z.-B.; Wang, G.-X.; Yan, X.; Wei, J.; Xi, Z. Construction of N-E bonds *via* Lewis acid-promoted functionalization of chromium-dinitrogen complexes. *Nat. Commun.* **2025**, *16*, 674.
69. Darani, F. A.; Yap, G. P. A.; Theopold, K. H. The Intrinsic Barrier for N≡N Bond Cleavage or Formation Mediated by the $Cp^*Cr(dmpe)$ Fragment Is Insurmountable. *Organometallics* **2023**, *42*, 1324–1330.
70. Uchida, K.; Kitayama, T.; Tanaka, S.; Adachi, S.; Iguchi, H.; Sakamoto, R.; Takaishi, S. High-Pressure Synthesis and Post-synthetic Elimination of N_2 Molecule of the Chromium Dinitrogen Complex, $[Cr(PCy_3)_2(CO)_3(N_2)]$. *Organometallics* **2025**, *44*, 459–463.
71. Kokubo, Y.; Tsuzuki, K.; Sugiura, H.; Yomura, S.; Wasada-Tsutsui, Y.; Ozawa, T.; Yanagisawa, S.; Kubo, M.; Takeyama, T.; Yamaguchi, T.; Shimazaki, Y.; Kugimiya, S.; Masuda, H.; Kajita, Y. Syntheses, Characterizations, Crystal Structures, and Protonation Reactions of Dinitrogen Chromium Complexes Supported with Triamidoamine Ligands. *Inorg. Chem.* **2023**, *62*, 5320–5333.
72. Kokubo, Y.; Igarashi, I.; Nakao, K.; Hachiya, W.; Kugimiya, S.; Ozawa, T.; Masuda, H.; Kajita, Y. The Steric Effect in Preparations of Vanadium(II)/(III) Dinitrogen Complexes of Triamidoamine Ligands Bearing Bulky Substituents. *Molecules* **2022**, 27, 5864.
73. Haynes, W. M.; Lide, D. R.; Bruno, T. J. *CRC HANDBOOK OF CHEMISTRY and PHYSICS*, 97th ed.; CRC Press, U.S., 2016.
74. Schneider, S.; Filippou, A. C. Triamidoamine Complexes of Chromium(III) and Chromium(IV). Inorg. Chem. 2001, 40, 4674–4677.
75. Evans, D. F. The Determination of the Paramagnetic Susceptibility of Substances in Solution by Nuclear Magnetic Resonance. *J. Chem. Soc.* **1959**, 2003–2005.
76. Sur, S. K. Measurement of Magnetic Susceptibility and Magnetic Moment of Paramagnetic Molecules in Solution by High-Field Fourier Transform NMR Spectroscopy. *J. Magn. Reson.* **1989**, *82*, 169–173.
77. Dolomanov, O.V.; Bourhis, L.J.; Gildea, R.J.; Howard, J.A.K.; Puschmann, H. OLEX2: A complete structure solution, refinement and analysis program. *J. Appl. Crystallogr.* **2009**, *42*, 339–341.

 doi:10.20944/preprints202512.1439.v1

78. Sheldrick, G.M. SHELXT–Integrated space-group and crystal-structure determination. *Acta Crystallogr. Sect. A Found. Adv*. **2015**, *71*, 3–8.
79. Sheldrick, G.M. A short history of SHELX. *Acta Crystallogr. Sect. A Found. Crystallogr.* **2008**, *64*, 112–122.
80. Hill, P.J.; Doyle, L.R.; Crawford, A.D.; Myers, W.K.; Ashley, A.E. Selective Catalytic Reduction of N_2 to N_2H_4 by a Simple Fe Complex. *J. Am. Chem. Soc.* **2016**, *138*, 13521–13524.